SMHI

Meteorologi

Nr 131, 2008

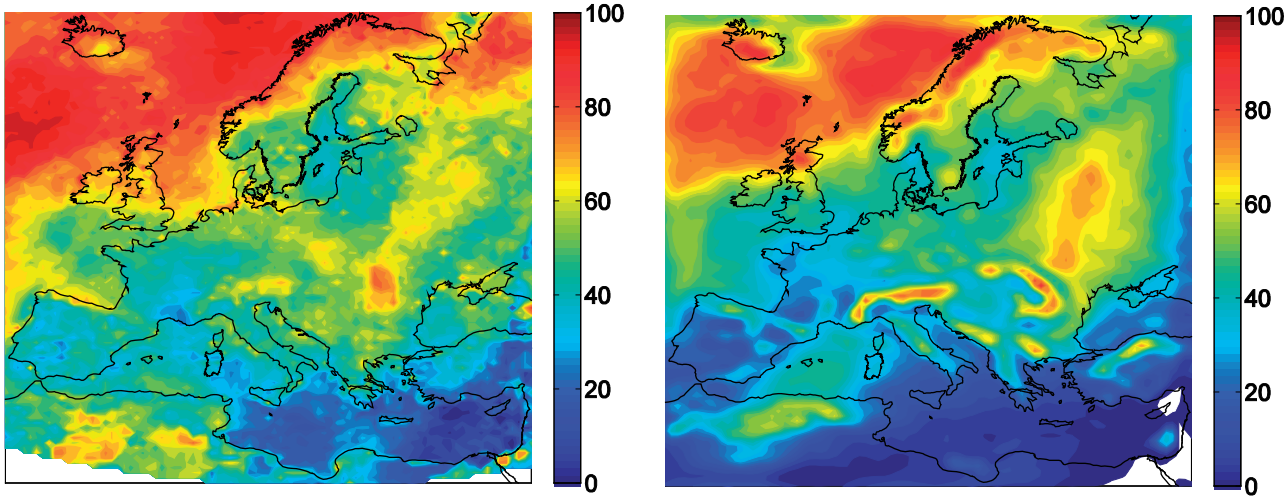

CM-SAF RCA

Preliminary use of CM-SAF cloud and radiation products for evaluation of regional climate simulations

Visiting Scientist Report
Climate Monitoring SAF (CM-SAF)

Ulrika Willén

Cover Picture: Plot of CM-SAF NOAA AVHRR-derived estimation of the Monthly Mean cloudiness and RCA simulated cloudiness in (%) for June 2006 over Europe.

Meteorologi
Nr 131, 2008

Preliminary use of CM-SAF cloud and radiation products for evaluation of regional climate simulations

Visiting Scientist Report
Climate Monitoring SAF (CM-SAF)

Ulrika Willén

Report Summary / Rapportsammanfattning

Issuing Agency/Utgivare

Swedish Meteorological and Hydrological Institute
S-601 76 NORRKÖPING
Sweden

Report number/Publikation

Meteorologi nr 131

Report date/Utgivningsdatum

April 2008

Author (s)/Författare

Ulrika Willén

Title (and Subtitle)/Titel

Preliminary use of CM-SAF cloud and radiation products for evaluation of regional climate simulations.

Abstract/Sammandrag

We have compared monthly mean cloud and radiation fields from the EUMETSAT Climate Monitoring SAF (CM-SAF, http://www.cmsaf.eu) data base with the clouds and radiation simulated by the Rossby Centre regional climate model (RCA) and by the European Centre Medium range Weather Forecast model (ECMWF) over Europe and North Africa for the time period January 2005 to December 2006.

ECMWF and RCA overestimate the cloud fraction by 20% over snow covered regions in the north east of Europe and overestimate the surface downwelling longwave radiation (SDL) by 20-40W/m^2 and surface outgoing longwave radiation by 10-30W/m^2. The RCA-simulated clouds have too much cloud water in northern Europe in summer and in autumn and they therefore reflect too much shortwave radiation at the TOA (TRS) and this also leads to an underestimation of the incoming shortwave radiation (SIS) at the surface. Over most of Europe and over sea ECMWF (all year) and RCA (in winter-spring) underestimate the cloud fraction which could explain a corresponding underestimate of TRS, overestimate of SIS and underestimate of SDL. The satellites overestimate cloud cover over sea due to problems in the treatment of sub-pixel cloudiness and therefore the models underestimates are larger over sea. Mainly RCA but also ECMWF overestimate cloud fraction on top of mountains and underestimate it along mountain ranges and have corresponding differences in the TOA and surface radiation fluxes compared to the CM-SAF data.

Over North Africa RCA underestimates TRS by -11W/m^2 and overestimates the TOA emitted thermal radiation (TET) by 8W/m^2. ECMWF underestimates TRS by -28W/m^2 and overestimates TET by 14W/m^2. These errors are similar to what has been found for many other global models and are attributed to clear sky errors either due to too high surface temperatures, errors in emissivity, albedo or lack of aerosols. Adding clear and cloudy skies radiation fluxes to the CM-SAF data base would help us to understand the reasons for ECMWF and RCA errors. The polar orbiting satellite retrieval for 2005-2006 erroneously overestimated cloud fraction over North Africa, which also affects the CM-SAF derived surface radiation fluxes.

Key words/sök-, nyckelord

CM-SAF, clouds and radiation, regional climate model, ECMWF

Supplementary notes/Tillägg

Number of pages/Antal sidor

48

Language/Språk

English

ISSN and title/ISSN och title

0283-7730 SMHI Meteorologi

Report available from/Rapporten kan köpas från:

SMHI
S-601 76 NORRKÖPING
Sweden

Contents

1 Introduction

The aim of this study has been to evaluate the usefulness of the Satellite Application Facility on Climate Monitoring (CM-SAF, http://www.cmsaf.eu) datasets for climate modelling development and validation. For model evaluation and improvement we need long-term homogeneous and consistent data sets, with large spatial coverage as is being collected by the CM-SAF. The interaction of moisture, clouds and radiation are crucial for the climate and its variability. Collocated measurements of these variables can help to reveal systematic biases in global and regional climate models simulations for present day and increase the confidence in climate predictions performed with the models.

CM-SAF is under development and many of the products will be further reprocessed in a near future. In this report we describe comparisons between the preliminary satellite data sets, and the simulated data sets from one regional climate model and one global Numerical Weather Prediction (NWP) model over the geographical domain of Europe and North Africa. We also give feedback that could contribute to improvements in the calibration and validation of the satellite data. The CM-SAF datasets are described in section 2 and the models in section 3. Results and discussions are presented in section 4 and the conclusions in section 5. Finally, plans for future work and comments are given in section 6 and 7.

2 Satellite data

The CM-SAF data is derived from both geostationary satellites and polar orbiting satellites with different instruments on board. This gives rise to differences in the derived variables such as cloud fraction depending on e.g. the viewing geometry (Johnston and Karlsson 2007). The cloud fractions in their turn are used in derivation of the surface radiation fluxes. We have used both types of satellite data in this study. In the following, we will denote products derived from polar orbiting satellites (such as NOAA and Metop) as PPS (Polar Platform System) products while products from the geostationary Meteosat platform are denoted MSG (Meteosat Second Generation) products.

The satellite data was obtained from the EUMETSAT Climate monitoring Satellite Applications Facility database (CM-SAF, 2007a) Monthly mean values of cloud fraction (CFC), cloud water path (CWP), surface incoming short wave radiation (SIS) and surface long wave radiation (SDL) and surface outgoing longwave radiation (SOL) are available from the polar orbiting NOAA satellites (from the AVHRR sensor) since January 2005 and from the METEOSAT Second Generation satellite (MSG, from the SEVIRI sensor), since September 2005 at 15km horizontal resolution. TOA fluxes, i.e., total reflected short wave (TRS) and total emitted long wave (TET) come from the Geostationary Earth Radiation Budget (GERB) instrument on board MSG with 45km horizontal resolution. The TOA flux products are global products where the area outside of the GERB field of view is covered by complementary information derived by the CERES instrument onboard the polar Aqua and Terra satellites. We have also used vertically integrated water vapour (HTW) from PPS (ATOVS instrument) at 45km and from MSG (SEVIRI) at 3 km resolution. The retrievals

have changed with time and the present CM-SAF data base therefore contains different versions. The CM-SAF variable names are summarised in Appendix 9.1 and the versions used for this study are given in Table 1 in Appendix 9.2. Later on (within the time frame 2010-2012) all the data will be homogenised and re-processed.

3 Models

The Rossby Centre Atmospheric regional climate model (RCA) is used for downscaling of climate change scenarios from GCM models. RCA is a hydrostatic gridpoint model with semi-Lagrangian dynamics originally based up on the numerical weather prediction model HIRLAM (Undén et. al. 2002). Most physical parameterisations have been replaced and the model has been developed to perform optimally in the 10-50km horizontal resolution range with 24 or 40 vertical levels (Rummukainen et. al. 2001, Jones et. al. 2004 and Kjellström et. al. 2005). Davies relaxation scheme (Davies 1976) is used to relax the RCA prognostic variables (pressure, winds, temperature and specific humidity) to the global model values in an eight-point boundary zone. The cloud water and diagnostic cloud fraction are set to zero at the boundaries.

To assess the cloudiness and radiation budget for present day climate, we have run RCA with ECMWF analysis on the boundaries. A regional model climate is largely determined by the driving model at the boundaries. In order to separate internal errors from boundary errors we have compared both RCA and ECMWF with the newly available CM-SAF satellite data. The horizontal resolution of RCA was 50km and 24 vertical levels. The ECMWF model for the period 2005-2006 had initially a horizontal resolution of 100km and 60 vertical levels but from March 2006 it was increased to 50km and 91 vertical levels. To obtain cloud fraction and radiative fluxes from the ECMWF model we used the 24 hours forecasts to allow for spin-up of the cloudiness (Allan et. al. 2007a). The ECMWF analysis and forecast fields were obtained from the MARS archives. In the following subsections, we will briefly describe the cloud and radiation parameterisations of RCA and ECMWF.

3.1 RCA

Cloud processes in RCA are separated into resolved clouds (large or mesoscale) and sub-grid scale (convective) clouds. The large scale clouds are described using the scheme of Rasch and Kristjánsson (1998). Convective clouds are represented with an entraining and detraining plume model using the approach of Kain and Fritsch (1993). The Kain-Fritsch scheme assumes that meso-scale circulations are resolved in the model and that only cloud scale fluxes have to be parameterised. The cloud fractions are determined diagnostically according to similar principles as those of Slingo (1987). The conversion of condensate into precipitation, follow the formulations used in cloud resolving models. There is only one variable for condensed water species and the distinction between water and ice phase is made as a function of temperature. The fraction of ice in the total condensate is

$$f_{ice} = 1 - \left(\frac{T - T_{ice}}{T_0 - T_{ice}} \right)^2 \quad (1)$$

where $T_{ice} = 250.16K$ and $T_0 = 273.16K$ are the thresholds between which mixed phase is allowed to exist, i.e. only ice for $T < T_{ice}$ an only water for $T > T_0$.

The radiation scheme in RCA is a modified version of the HIRLAM radiation scheme, developed originally by Savijärvi (1990) and Sass et. al. (1994) for NWP purposes. The scheme is computationally fast but highly simplified with only one wavelength band for the longwave region and one for the shortwave region. The LW part is an emissivity-type broadband scheme. Initially only H_2O line absorption was treated explicitly. Räisänen et. al. (2000) introduced explicit H_2O continuum and CO_2 absorption in RCA. The cloud fraction given as output from RCA is calculated assuming maximum-random overlap but in the radiation calculations one assumes maximum overlap, i.e. less cloud cover, due to computational reasons.

3.2 ECMWF

The European Centre for Medium range Weather Forecast model (ECMWF) documentation can be found on http://www.ecmwf.int/research/ifsdocs. Cloud and large-scale precipitation processes are described by prognostic equations for cloud liquid water and ice and cloud fraction and diagnostic relations for precipitation. The division into liquid and ice water is the same as for RCA in Equation 1. The scheme is described in detail in Tiedtke (1993). Cumulus convection is parameterized by a bulk mass flux scheme which was originally described in Tiedtke (1989). The scheme considers deep, shallow and mid-level convection. Clouds are represented by a single pair of entraining and detraining plumes which describes updraught and downdraught processes. Momentum and tracer transport is also included.

The ECMWF radiation scheme for 2005-2006 included the ECMWF-RRTM LW scheme (Mlawer et. al 1997, Iacono et. al. 2000, Morcrette 2002) and a SW scheme originally developed by Fouquart and Bonnel (1980). The ECMWF-RRTM LW spectrum is divided into 16 bands for clear and cloudy sky calculations. The shortwave region is divided into six bands with three bands in the near infrared and visible part, respectively. Maximum-random overlap is assumed for multiple cloud layers in the LW and SW regions.

The ECMWF model being a NWP model is constantly being updated and improved which can affect the performance and comparison with observations. Here we list the model changes that have occurred during 2005-2006 which could affect the clouds and radiation (http://www.ecmwf.int/products/data/technical/model_id/index.html). Initially, for this time period the cycle version was CY28r3 (from 28/9/2004). In CY29r1 (from 5/4/2005), a new moist boundary layer scheme was introduced that generated better low level clouds in European winter anticyclonic conditions. For CY29r2 (28/6/2005) there were humidity analysis changes affecting the spin-up and stratosphere and convection changes, which lead to some improvement in rainfall forecasts over Europe. Further in CY30r1 (1/2/2006), there was

an increase in horizontal resolution to T799 (about 50 km for Europe) and an increase in vertical resolution to 91 levels (before 60) and the model top was raised to 0.01 hPa. This lead to improvements in precipitation scores over Europe, in particular for large daily rainfall amounts. Finally, in CY31r1 (12/9/2006), there were revisions of the cloud scheme, including treatment of ice supersaturation and new numerics, and implicit computation of convective transports. There were also an introduction of turbulent orographic form drag scheme and revision to sub-grid scale orographic drag scheme and a gust fix for orography and stochastic physics. These changes also led to improved precipitation forecasts over Europe according to the ECMWF webpage.

4 Results and discussions

The satellite data and the ECMWF data have been interpolated to the RCA grid of 50km horizontal resolution (Figure 1, Appendix 9.3) to enable the comparison. We have compared two years of model and satellite data from January 2005 until December 2006. The ECMWF radiation fields were only available until August 2006. The model radiation fluxes monthly means are calculated from all model time steps while the moisture parameters, cloud fraction, cloud water and specific humidity are calculated from the 6 hourly instantaneous values. The time period is too short for a statistically significant validation of the monthly means, still some features stick out even if we consider the inter annual variability as will be shown in this section.

We have included many figures in this report in order to give as much feedback as possible to the CM-SAF team and we present them all in the Appendix 9.3. There we show 2D plots of the monthly mean values and the biases in CFC, CWP, HTW, TRS, SIS, TET, SDL and SOL comparing MSG, ECMWF and RCA with PPS for different months of the year (Figures 2-12). We have also calculated the model and satellite mean values, the bias, the standard deviation (std) and the correlation between the models and PPS for three land regions and two sea areas; for land points north of 55°N (North Europe: L1), land points between 36°N and 55°N (middle Europe: L2), land south of 36°N (North Africa: L3), for sea points north of 43°N (the Atlantic: S1) and sea points south of 43°N (the Mediterranean Sea: S2) from January 2005 to December 2006. These areas are indicated with lines in Figure 1 and the results are shown in Figures 13-21 in the Appendix 9.3. The reason for dividing the model area into smaller parts is to avoid cancelling of errors and to try to separate the errors depending on the geographical location, the surface type and the season. For a future study it would be good also to single out snowy, mountainous (high altitude) and desert regions as will be discussed below. The mean values, the bias and the standard deviation and the correlation between the models and the PPS data for all variables are summarised in Table 2-10 in the Appendix 9.2. Since we only had 15 months of MSG data we have not calculated the mean statistics for MSG for the different regions. We have excluded the 8-point RCA boundary zone in the calculations and in the figures. In the following subsections we present the results and discussions for all the variables.

4.1 Fractional Cloud Cover (CFC)

According to the CM-SAF validation reports (e.g. CM-SAF 2005) the cloud fraction product should be the most well-tuned and reliable of the CM-SAF cloud products being within the target accuracy of 10%. The best skill is found over central Europe. Moving northwards, across the Nordic region towards the Arctic, the quality degrades slightly especially for MSG since the CFC is larger in the northern part of the common area, due to the increasing viewing angle (Johnston and Karlsson 2007). Figure 2 show the cloud fraction for PPS, MSG, ECMWF and RCA for four different months through out the two years. We see that the large patterns of the model and satellite cloud cover agree, such as the land sea contrast and the seasonal cycle with less cloud cover in summer and more in winter. Figure 4 show the differences between MSG and PPS and the models compared to both PPS and MSG data. Figure 13 show the mean, bias, standard deviation and correlation between the models and PPS, and between MSG and PPS, for the five different regions as function of time. The mean statistics for 2005-2006 for those regions are given in Table 2. The most pronounced differences between the models and satellite data are found over sea, North East (NE) Europe in winter, mountains and North Africa as will be discussed below. First we note some technical issues and discuss the difference between the two satellite data sets.

There are unrealistic linear boundaries in the results from north (starting at 45°E) to south (finishing at 20°E) in PPS CFC for April-August 2006 (e.g. June 2006, Fig 2 and Fig 4). This is an artificial feature caused by different coverage of NOAA AVHRR overpasses in the different processing regions (or tiles) applied in the CM-SAF processing chain. This problem will be solved in the near future (2008 or 2009) by changing the processing mode (leaving the tiling approach to process on full AVHRR overpasses) and by utilising a distributed dataset (EARS-AVHRR) with AVHRR data from several European HRPT stations (K-G Karlsson, SMHI personal communication). MSG has very large CFC values in January 2006 (Fig 13) which should be further analysed. As mentioned earlier, RCA cloud fraction and cloud water is set to zero at boundaries. Even if we do not plot the outer most eight boundary points, it is still noticeable that the cloud fraction for RCA goes toward zero near the boundaries (Fig 2) which will affect the radiation fields.

Comparing the two satellite data sets, we see that MSG has more CFC than PPS (except south of 44°N) and MSG increases northwards as expected from the viewing angle (Fig 4 row 1 and Fig 13b,13n). Johnston and Karlsson (2007) also found a large difference comparing cloud fraction from MSG and PPS. The difference was reduced when they included all cloud contaminated pixels for both PPS and MSG that can arise due to fractional and thin clouds. They suggest more work should be done finding the best technique for how to include such pixels (i.e., how to estimate sub-pixel fractional cloud coverage). Over North Africa and other dry regions the present PPS version (1.0) has high and unrealistic cloud amounts (20% to 40% more than MSG), due to problems separating desert regions from low level clouds (e.g. Johnston and Karlsson 2007). This was improved in the latest PPS version (1.1) for data from January 2007 but it is not yet available for older CM-SAF data. In general there is also more CFC for MSG than PPS over sea, except for some parts over the Mediterranean Sea and the Bay of Biscay. The difference in CFC over sea is larger in the north particularly in spring as can be noticed over the lakes in Finland, the Baltic Sea and the Barents Sea (see MSG-PPS March 2006 Fig 4). The main reported bias for the satellite derived cloud fraction in the CM-

SAF validation reports (CM-SAF 2005 and 2007b) is an overestimation of cloud fraction above sea of 10% compared to synop for both PPS and MSG.

Comparing the models with the satellite data over the North Sea and the Atlantic we find that ECMWF and RCA have less cloud cover than both PPS and MSG (Fig 4 and Fig 13n) with a larger difference in winter. ECMWF and RCA underestimate the CFC over sea compared to PPS by -20% in winter and -10% in summer (mean bias ECMWF S1 -12% and RCA S1 -16%, respectively, Table 2). The difference compared to MSG is larger, -25% in winter and -15% in summer. Over the Mediterranean Sea the models underestimate the CFC by -25% in winter and -10% in summer compared to PPS and MSG (Fig 13r), the mean S2 bias is -17% for ECMWF and -18% for RCA. The satellites have a much sharper land sea gradient than the models and since they also have much more cloud fraction than synop (10%) and than the models as we found in this study (10%-25%), this indicates that the satellite overestimate of cloud fraction over sea is possibly larger than the target accuracy of 10%.

Similarly over land in mid and south Europe ECMWF and RCA have less cloud fraction than PPS and MSG (Fig 13f, L2 mean bias ECMWF -7% and RCA -6%, Table 2). Since the satellites might underestimate CFC over land according to CM-SAF (2007b) this could mean the models underestimates are even larger. This was found when ECMWF (ERA40, version cycle23r4, Uppala et. al. 2005) and RCA were compared to CRU and ISCCP cloud cover for the period 1985-1989. RCA and ECMWF underestimated CFC compared to ISCCP by -15% and compared to CRU by -10% (not shown). Note that the underestimation of CFC for RCA could also be larger since maximum overlap is applied in the radiation calculations which give a smaller effective cloud fraction than is shown in Figure 2.

RCA, ECMWF and MSG overestimate the cloud cover over NE Europe and Scandinavia compared to PPS during winter and spring (Fig 4, Fig 13b). ECMWF, RCA and MSG have positive biases of up to +20% to 40%. The overestimate take place over areas that are snow covered in the models as shown in Figure 3. Since one could expect a small but noticeable underestimation over land for the winter season by the PPS method due to lost (or even inversed) contrast between cloudy and cloud free areas in infrared imagery (CM-SAF 2005), this could perhaps partly explain the overestimate by the models. Further, the difference between PPS and MSG could be due to the viewing angle and different sensitivities to the surface reflectance. However, RCA and ECMWF (ERA40) also overestimate the cloud fraction compared to ISCCP data by 15% and compared to CRU (Mitchell and Jones 2005) by 10% in this region for the time period 1985-1989 (not shown). If it is the models and MSG overestimating cloud fraction or if it is PPS having problems over snow covered land in winter we will return to in section 4.6.

On top of mountains (the Scandinavian range, the Alps and the Sierra Nevada) RCA has a large positive bias in CFC of 20-40% and ECMWF 10-20% compared to PPS, respectively. Along and prominently on the leesides RCA have underestimates of -10% to -20% and ECMWF -5% to -10% compared to PPS. Karlsson et. al. (2008) found that RCA overestimates cloud fraction over the Scandinavian range and underestimate the leeward minima compared to the SCANDIA satellite climatology for 1991-2001. We also find that RCA has similar biases compared to ISCCP and CRU for 1985-1989 (not shown). Compared to MSG cloud fraction the RCA biases are similar but weaker due to the higher values of

cloud fraction for MSG. The overestimate of cloud fraction on top of mountain ranges and underestimate on the leeside could be connected to problems with the orographic flow in RCA. We believe the local winds are underestimated and the winds over the mountains are overestimated as was found in the PYREX experiments for a number of models including RCA/HIRLAM (Georgelin et. al. 2000 QJRMS). This could lead to too much humidity on top of the range and therefore to high cloud amounts and also too much suppression of clouds on the leeside. Other contributing factors to the high CFC could be the horizontal diffusion of humidity becoming vertical at steep orography and the neglect of advection of precipitation in RCA. Previous versions of ECMWF also had problems with the flow over mountain ranges and the surface roughness was increased to artificially compensate for this. The changes in the ECMWF orographic drag scheme in September 2006 appears to have reduced the maxima over mountains for October-December 2006 compared to the same time period 2005 (not shown). A sensitivity test increasing the maximum roughness length over mountains in RCA from 15 m to 100 m as in ERA40 did reduce the cloud fraction maxima on top and decreased the minima leeward somewhat (not shown). Further work with the orographic parameterisation is needed in RCA. In addition to the model orography problems, it could also be the satellites underestimating the cloud fraction over high altitude (snowy) regions as we will return to in section 4.5

Over North Africa the models agree fairly well with MSG except over the Atlas mountain range where RCA and ECMWF overestimates of CFC are visible as over the European mountains. PPS has much more CFC (30%) than MSG and the models, as expected due to the problems for the PPS retrieval before January 2007. The errors in PPS-CFC will also affect the derived surface radiation fluxes as shown later in section 4.4-4.6.

We have only discussed the biases in cloud cover so far. Figure 13 show that the standard deviations and correlations are similar for ECMWF and MSG compared to PPS. MSG is closer to PPS in winter and does not have the seasonal variation in bias, std and correlation as ECMWF and RCA. For North Europe (region L1), ECMWF and RCA standard deviations are worse in winter and the correlations are even below zero due to the differences in the NE snowy part. The MSG and PPS differences are almost as large as the ECMWF and PPS differences. Since ECMWF is a forecast model and we have used the short term forecasts this model should be close to observations. Still we would hope that the differences between MSG and PPS can be minimized in order to trust the satellite measurements more. Comparing RCA with ECMWF statistics we see that the RCA standard deviation is larger and the correlation smaller for all regions, even if the seasonal variations are similar. Since RCA is run in climate mode without data assimilation we expect worse scores for RCA. However, identifying any large deviations compared to ECMWF or the satellite estimates will help us improving our regional climate model.

4.2 Cloud water path (CWP)

The cloud water path for the CM-SAF data is calculated from the satellite retrieved cloud optical depth (COT) and the effective radius (R_e). The retrieval is less reliable for thick clouds with COT>50 and for thin clouds with COT<8 for which climatological R_e are used. Any errors in COT will affect the CWP. According to CM-SAF (2005) the most serious weakness of the version of COT used for 2005-2006 is the inability to compensate accurately for

varying surface reflectivities. For semi-transparent clouds overlying surfaces with high reflectance the optical depth and subsequently CWP will be largely overestimated. Later versions (from autumn 2007) use surface reflectivity maps which can reduce the problem. According to CM-SAF (2005) CWP from PPS (AVHRR) fulfill the target accuracy of 15%, having been validated with ground based Micro Wave Radiometers (MWR) for overcast skies and clouds with CWP<800 g/m^2. MSG (SEVIRI) retrievals have been found to significantly underestimate CWP by -10 to -40 g/m^2 and have large variances compared to MWR (CM-SAF 2005). However, it has later been shown that uncertainties and errors in the calibration constants for visible and near infrared channels are able to explain a large part of the difference. Roebeling et. al. (2007) have evaluated a later upgraded version of the MSG CWP retrieval algorithm (making use of calibration corrections derived from comparisons with MODIS channels and collocation of SEVIRI and AVHRR measurements near the MSG sub-satellite point) and found that during summer, the instantaneous LWP retrievals from SEVIRI agreed well with those from the MWRs. The accuracy is better than 5g/m^2 and the precision is better than 30g/m^2. During winter, SEVIRI generally overestimates the instantaneous CWP values compared to MWR, the accuracy drops to 10g/m^2 and the precision to about 30g/m^2.

The CWP satellite products are only made for daytime conditions (need visible radiances for derivation) and at least two scenes per day are required (most critical for PPS). Here, we have compared with the model monthly fields calculated from 6 hourly instantaneous values. In order to make a better comparison we should preferably select the model data for the same times as the satellite data. This could be done if that information also is kept in the CM-SAF data base. If that is not feasible, at least for later studies, we should only compare with model daytime values to improve the comparison, especially in summer.

Despite the mismatch of the model and satellite timings and the preliminary state of the MSG CWP products we have compared the models and MSG with PPS in Figures 5 and 14. We note that PPS has much more cloud water than MSG in north of Europe and over mountains especially in winter. The current available MSG product is the old erroneous version with very small CWP values. We also note that the PPS data in January-March 2005 (corresponding to version 130 in the CM-SAF data base, Table 1) have unrealistically large values for all areas (Fig 14). ECMWF and RCA also underestimate CWP in winter-spring compared to PPS over land, particularly over eastern parts of Europe. The models (and MSG) underestimates of CWP over the Scandinavian mountains and the Alps and the north east snowy region (-200 g/m^2 less CWP than PPS) are probably linked to the erroneous overestimation of CWP by PPS over high reflectance surfaces. ECMWF CWP is fairly similar to PPS for the rest of the year with slightly more CWP over the Atlantic and somewhat less over the Mediterranean. Over North Africa the ECMWF and PPS cloud water values are similar but RCA has an overestimate in winter compared to PPS and ECMWF.

The most pronounced feature for RCA is that it has much more CWP than the satellites and ECMWF from April till October by more than 200g/m^2 (i.e. a factor 2-3) in northern half part of the area (Fig 5). Still the bias pattern for RCA-PPS is similar to that of ECMWF-PPS even if the values are much higher. The RCA bias in CWP is also obvious over sea and is much larger for the Atlantic than for the Mediterranean (mean bias 183 and 28 g/m^2, Table 3). Older versions of RCA had problems with excessive drizzle. A number of changes were made in the cloud parameterisations among them the auto conversion threshold was increased in order to reduced the drizzle (Kjellström et. al. 2007). Unfortunately, this led to large cloud water

amounts instead as has been found in other studies (Van Lipzig et. al. 2005, Schröder et. al. 2006 and Illingworth et. al. 2006, Karlsson et. al. 2008). A sensitivity experiment was made for this study reducing the auto conversion threshold to its original value. This gave reduced cloud water and somewhat better solar radiation fluxes (not shown). We need to improve the amount of cloud water in the model and plan to utilise more physically based auto-conversion parameterisations in RCA. Some of the bias in RCA cloud water could be due to the diagnostic divisions into cloud ice and cloud water made in RCA and ECMWF mentioned in section 3. However, comparing the total cloud water content for both RCA and ECMWF with CM-SAF give similar results, since in summer when the largest bias takes place, most of the cloud water content is in the water state.

Figure 14 shows that the standard deviations and correlations for CWP are similar for ECMWF and MSG. In winter ECMWF, RCA and MSG standard deviations are high and the correlation low and even below zero due to the large difference over mountains and snowy regions compared to PPS for all of Europe (region L1 and L2). In summer ECMWF and MSG have much smaller standard deviations and higher correlations. The large amount of CWP for RCA in the summer half give rise to much larger standard deviations (RCA 80g/m^2 and ECMWF 10g/m^2) while the correlation is just somewhat lower than for ECMWF due to the similar bias patterns. The correlation for sea varies from month to month and is less than 0.5 for the Atlantic and less than 0.7 for the Mediterranean Sea for both ECMWF and RCA.

4.3 Vertically Integrated water vapour (HTW)

We have compared the vertically integrated water vapour from the models with PPS (ATOVS) HTW product in Figures 6 and 15. The PPS data is available from September 2005 until August 2006 from the CM-SAF data base (stopped in August 2006 due to technical problems). MSG (SEVIRI) data is also plotted but it has poor quality according to the CM-SAF validation reports. ATOVS has higher accuracy in the lower atmosphere and is used for reference in a merged PPS and MSG product which we have not looked at. PPS-ATOVS has higher uncertainty over land than sea. The CM-SAF target accuracy for integrated water vapour is 1.5 kg/m^2.

Over the Atlantic ECMWF and RCA overestimate HTW by 1-2kg/m^2. This is similar to what was found by Allan et. al. (2004) over midlatitude oceans, where ERA40 overestimate moisture by up to 1-3kg/m^2 compared to satellite (SSM/I and SMMR) measurements. MSG has much larger values than PPS over sea by 5-15 kg/m^2. Over land we see large and negative differences for the models compared to PPS. The models (and MSG) have more structures e.g. over mountains where the models and MSG have minima, which can not be seen for ATOVS. The orographic information was missing in this preliminary ATOVS HTW product. New correct reprocessed data is now available from CM-SAF (Jörg Schulz, DWD personal communication). Also the models have negative biases compared to PPS in summer of up to -10 kg/m^2 over Africa and Spain (L3 mean bias -3kg/m^2, Table 4) due to the very large values for ATOVS >35kg/m^2. Over southern Europe and North Africa MSG has less water vapour than PPS (-5 to -15kg/m^2) as seen in Figure 6 (second row). According CM-SAF (2007b), validation of ATOVS level-2 products indicated algorithm problems over desert areas where ATOVS shows a positive bias in HTW when compared to radisonde data. Over deserts SEVIRI water vapour has too low values when compared to estimates from other satellites

and ECMWF model output according to CM-SAF (2007b). This is due to an insufficient description of the emissivity of desert surfaces in the infra red.

The correlations between ECMWF and RCA with PPS are very high and close to one over North Europe and the Atlantic in Figure 15d and 15p, but lower for MSG compared to PPS (0.5 and 0.8 respectively). Over Africa the model and MSG correlations are equally bad compared to PPS. Due to the problems with the satellite estimates and the short time period we can not draw any conclusions from the HTW comparison and have to await later versions.

4.4 TOA Reflected Solar (TRS) and Surface Incoming Solar (SIS) radiation

We present the results for the solar radiation fields at the TOA and surface together in this section since errors in TRS and SIS are often anti-correlated with each other and correlated or anti-correlated with CFC and CWP errors. The CM-SAF TOA monthly mean TRS flux has an accuracy of 4.7W/m^2 (for version 120, Table 1), which is well within the target absolute mean error of 10W/m^2 according to CM-SAF (2007c) The surface solar fluxes from PPS and MSG are expected to meet the target accuracies of 10W/m^2 according to CM-SAF (2005), despite PPS had some problems with large positive biases for certain months. For the surface fluxes, one would expect larger errors than at the TOA since a multiple of information is needed in their derivation. Input data for SIS is the TOA albedo from GERB, water vapour from GME (Global Modell Europa from Deutsche Wetterdienst, Majewski et. al. 2002), aerosol climatologies and satellite estimates of CFC and surface albedo (SAL) from SEVIRI or AVHRR. When analysing the fields we need to consider any NWP model changes and errors in CFC and SAL that can give errors in SIS, such as the reported overestimate of CFC over sea and over North Africa. We also note that there is a large difference in surface albedo over snowy terrain for the two satellite data sets as pointed out in CM-SAF (2007b). MSG SAL is much larger over mountains than AVHRR, which could be due to the viewing angle for snow-covered surfaces, possibly affecting the two derived surface solar fluxes.

The TRS from CM-SAF MSG and the biases for ECMWF and RCA are plotted in Figure 7. Mean values of SIS for PPS and MSG and the biases for the models compared to both PPS and MSG are shown in Figure 9. Timeseries for the mean, bias, standard deviation and correlation are shown in Figures 16 and 18 and mean values for the two years are given in Table 5. Over most of the model area ECMWF (all year) and RCA (in winter-spring) underestimate TRS by -10 and -5 W/m^2 (Fig 7, row 2 and 3 and Fig 16b and 16f). The models also overestimate SIS compared to both PPS and MSG, with the largest overestimate compared to MSG-SIS in winter and spring of up to 30W/m^2 (Fig 9 row 4-7 and Fig 18b and 18f). This is possibly linked to the previously discussed underestimation of the cloud fraction by the models compared to PPS and even more so compared to MSG over both sea and land (e.g. Fig 13f) except for the NE corner.

According to Allan et. al. (2004) ERA40 underestimates the clear-sky TRS over NH land compared to NCEP and ScaRaB, suggesting the ERA40 albedo is too low. ERA40 absorbs too much solar radiation for clear skies throughout the year, despite the surface albedo over high-latitude forest was improved in ERA40 (Simmons 2001). The underestimates we see in

all-sky TRS for ECMWF might therefore also be due to clear-sky errors and not just due to the CFC underestimations as we suggest here.

Over mountains both in Europe and North Africa where the models (mainly RCA) have more clouds than PPS and MSG, there is an overestimate of TRS and underestimate of SIS on top of the ranges and the opposite along the ranges where the models have less clouds, i.e. an underestimate of TRS and overestimate of SIS.

Over North Africa ECMWF and RCA underestimates TRS all year (RCA mean bias L3=-11 W/m^2, ECMWF mean bias L3=-28 W/m^2). Other studies report similar biases over North Africa and have attributed them to clear-sky errors. Allan et. al. 2004 found that ERA40 underestimates clear-sky TRS by more than 15 W/m^2 compared to satellite data which was consistent with NCEP clear-sky TRS errors, which Yang et. al. 1999 attributed to an underestimation of surface albedo. Allan et. al. (2007b) also found that MetOffice global NWP model underestimates TRS in North Africa. Other reasons for the TRS underestimates could be lack of aerosols or too low humidities making the models too transparent in the short wave region. In order to try and understand the model errors in our study, we would like to compare clear and cloudy sky separately and the aerosol climatologies and albedo distributions. There are also large overestimates in SIS for the models and MSG compared to PPS-SIS (RCA and ECMWF mean biases L3=33 W/m^2) which probably are linked to the erroneous large PPS-CFC over this region which will affect the PPS derived radiation fields giving too low SIS.

The CM-SAF CWP product is more preliminary than the CFC product but we can note that the RCA and ECMWF solar flux biases are similar for times and regions where the model CWP amounts are similar like in winter and spring in Figures 5, 7 and 9. The most pronounced difference in TRS and SIS between RCA and the CM-SAF data and ECMWF occurs in summer-autumn. RCA overestimates TRS (mean bias L1=5W/m^2, L2=10W/m^2, max bias L1 and L2 50W/m^2) and underestimates SIS (mean L1=-13W/m^2, L2=-1W/m^2, max L1 -50W/m^2 and L2 -10 W/m^2) due to the large overestimation of cloud water by RCA (e.g. Fig 5 row 4). Similarly over sea RCA overestimates TRS in summer half (mean S1=5W/m^2, S2=5W/m^2 max S1 and S2 30W/m^2) and underestimates SIS (mean S1=-21W/m^2, S2=0.5W/m^2, max S1 -40W/m^2 and S2 -5 W/m^2) which also are linked to the overestimation of cloud water. In areas where RCA cloud fraction is underestimated compared to the MSG cloud fraction the overestimate in CWP does not affect TRS as much as can been seen in the northern part of the region near the boundary zone and on the lee-side of mountains (e.g. compare September 2005 or June 2006 in Fig 4 row 5, Fig 5 row 4 and Fig 7 row 3). In the sensitivity experiment reported in section 4.2, reducing the CWP amounts for RCA also reduced the TRS and SIS errors (not shown).

The ECMWF and RCA standard deviations and correlations for TRS and SIS follow the same patterns but are worse for RCA (Fig 16 and Fig 18). In the northern part (L1 and S1) in summer, the correlation for RCA is less than 0.4 and the standard deviation more than 20W/m^2. Over middle Europe (Fig 16h) mainly RCA but also ECMWF TRS correlations have a semi-annual pattern with worse correlation (0.6) in spring and autumn and better in summer (0.9). For North Africa the mean ECMWF and RCA TRS standard deviations are 15 and 18 W/m^2, respectively.

4.5 TOA Emitted Thermal (TET) and Surface Downwelling Longwave (SDL) radiation

Here we present the TOA and surface longwave radiation fields and discuss the correlations with the cloud errors. The CM-SAF TET monthly means have an accuracy of 5W/m^2 with the largest measured systematic error occurring for desert scenes (CM-SAF 2007c). The targeted accuracy of 10W/m^2 for SDL is also expected to be met (CM-SAF 2005). SDL is calculated using the algorithm by Gupta (1989) and Gupta et. al. (1992) assuming a linear relationship between the clear-sky flux and the flux in cloudy situations. The PPS or MSG cloud fraction, cloud top height and a fixed cloud thickness are used together with temperature, humidity profiles and HTW from the GME model. There could be errors or inconsistencies in the derived SDL due changes in the NWP model or problems for the satellite retrieved cloud fraction or cloud top height for certain regions or seasons.

Figures 8 and 17 show the differences in TET and Figures 10 and 19 the differences in SDL between the models and the CM-SAF data. All year ECMWF overestimates TET and underestimates SDL by 10-20W/m^2 over regions where the cloud fraction is underestimated, except in NE Europe in winter where the cloud fraction is overestimated and the bias in TET is close to zero. The ECMWF TET and SDL biases over sea are larger than over land and have clear seasonal cycles with the largest overestimate for TET and underestimate for SDL in winter-spring when the CFC bias is largest. However, as mentioned in section 4.1, the satellites probably overestimate the cloud fraction over sea resulting in too much SDL for the CM-SAF products since CFC is used as input and therefore the model underestimate might be less than shown here. Allan et. al. (2004) found that ERA40 overestimates all-sky TET which they state is due to an underestimation of cloud ice over the Extra tropics (Chevallier 2005) and not due to the cloud fraction as we suggest here. We need to look at the radiation budgets for clear and cloudy skies separately and compare with other cloud fraction observations especially over sea to help to understand how large part of the long wave errors are due to the models and the satellites, respectively.

The cloud fraction and long wave errors are less correlated for RCA than for ECMWF. Over mid Europe RCA TET mean bias is close to zero (Fig 17f) and the SDL bias is also close to zero (Fig 19f), even if the CFC is underestimated (Fig 13f). Over sea RCA TET and SDL biases are close to zero over the Atlantic (Fig 17n,19n) and the TET bias is positive and the SDL bias is negative over the Mediterranean (Fig 17r,19r), despite RCA underestimates CFC by 20% over both areas (Fig 13n,13r). The empirical formula in RCA for clear-sky cooling beneath clouds has been modified in the current version leading to increased SDL beneath clouds (and indirectly decreased TET). The shift between RCA and ECMWF in TET and SDL over the Atlantic is 20W/m^2 while over the Mediterranean it is only about 5W/m^2. The reason there is more difference for the Atlantic than for the Mediterranean is probably due to the much larger mean values of cloud fraction (RCA S1 mean 66% and S2 mean 32%, respectively) i.e. the change in cooling beneath clouds in RCA affects the long wave flux much more over the Atlantic than over the Mediterranean.

The errors in CWP, such as the large overestimates by RCA in spring and summer, do not appear to be strongly correlated with the long wave errors, as was found for the SW errors in

the previous subsection. The clouds are probably already black in the LW and therefore the amount of cloud dominates over the cloud water content in the LW calculations.

For the NE corner of Europe where we found an overestimation of cloud fraction in winter, there is an overestimate of SDL for ECMWF and RCA compared to PPS by 20-40 W/m^2 and to MSG by 10-20 W/m^2. The bias in TET for this region is close to zero for ECMWF and negative for RCA (-20 to -40W/m^2). According to Allan et. al. (2004) ERA40 overestimates clear-sky TET and has a warm bias over regions in Europe (all Northern Hemisphere land) in winter, which might have resulted from an overcompensation from too cold temperatures and underestimation of TET as found for ERA15 (Simmons 2001). We believe the difference in TET biases could be due to ECMWF having enough clouds just compensating for the clear sky overestimate of TET (as found by Allen et. al. 2004) while for RCA we also have more SDL wave beneath clouds (due to the change in cooling) so the overestimate of CFC by RCA will further increase the underestimate in TET.

The mountain ranges are obvious in the TET bias for RCA (and for ECMWF), with too little TET on top and too much along (especially on lee-sides) and the opposite occur for SDL with too much on top and too little along which again we believe is coupled to the CFC errors. The errors are anti-correlated with the SIS and TRS errors found in section 4.4. Comparison of satellite derived SDL with in situ measurements (CM-SAF 2007b) show average mean absolute errors ranging from 6 to 10% and underestimates for mountains with a relative large bias for Payern (Payern -20.7% in December 2004). These errors are thought to be due to model altitude and measurements differences. But from our results we suggest it could be at least partly real CM-SAF underestimates of SDL due to an underestimation of CFC. Comparing clear and cloudy skies separately also for the standard CM-SAF validations would help to clarify if this is the case.

Over Africa ECMWF and RCA overestimate TET by 20-30W/m^2 all year (anti-correlated with the TRS errors) and there are SDL underestimates of 5W/m^2 compared to SDL from MSG. The models and MSG largely underestimates SDL (-40W/m^2) compared to PPS. However, we believe this is due to the erroneous PPS overestimate of CFC (30%) which is used in the derivation of SDL and we will not discuss PPS-SDL further. The model and MSG cloud fractions are very similar over North Africa therefore we do not believe the radiation errors are due to CFC errors but they could be due to errors in humidity, emissivity or aerosol properties. Other studies have found similar errors in TET and have attributed them to clear-sky problems. Allan et. al. (2004) found that ERA40 overestimates TET over North Africa compared to satellite data by 15W/m^2, due to more clear-sky TET. This was also found by Allan et. al. (2003) for the Hadley Centre atmospheric climate model (HadAM3) compared to ERBS data over this region. Similar errors in TET were found for NCEP by Yang et.al. (1999), they attributed the differences to an overestimation of surface emissivity or temperature. Slingo et. al. (1989) found that ERA15 overestimates clear-sky TET over north Africa and attributed the discrepancy in July to overestimations in ERA15 surface temperature based on comparison with surface observations. Finally, Allan et al (2007b) attributed the Met Office global NWP model TET errors partly to unrealistic surface emissivities but mainly due to lack of mineral dust. We need further analysis to understand the ECMWF and RCA differences compared to MSG over desert regions, the first step would again be to separate the comparison into clear and cloudy skies and to compare the emissivities.

Also for the TET and SDL the ECMWF and RCA standard deviations and correlations follow the same patterns, being slightly worse for RCA (Fig 17 and Fig 19). The RCA TET and SDL standard deviations are about 10W/m^2 while for ECMWF they are 5W/m^2. The ECMWF TET and SDL correlations are close to 1 while the RCA correlations are about 0.9, being worse in the north (where CFC is overestimated) and in spring over the Atlantic for TET. This last problem could be due to the change of sign of the biases for RCA near the boundary zone which we will look further into. Over North Africa the RCA TET bias is smaller than for ECMWF although the standard deviation is larger and the correlation somewhat lower than for ECMWF.

4.6 Surface Outgoing Longwave radiation (SOL) and surface skin temperature (T_s)

Finally, we will compare the CM-SAF surface outgoing longwave products with the model longwave fluxes. CM-SAF SOL is calculated using the skin or surface temperature, T_s, from the GME model according to

$$SOL = \varepsilon \sigma_b T_s^{\,4} \qquad (2)$$

where ε is the emissivity σ_b the Boltzman constant. The emissivity for the MSG product is assumed to be 1 everywhere and for PPS it is taken from CERES/SARB (http://www-surf.larc.nasa.gov/surf/pages/emiss.html) according to Richard Müller and Rainer Hollman (DWD). SOL is also expected to meet the target accuracy of 10W/m^2 (CM-SAF 2005), which corresponds to an accuracy of about 2K in T_s.

Figure 11 show the PPS and MSG SOL and the difference plots for MSG, RCA and ECMWF compared to PPS and MSG and Figure 20 show the corresponding timeseries. Despite the same temperature input MSG and PPS SOL products are different by -1 to 30W/m^2 for certain regions and times. The small negative differences must be due to the different temporal sampling for the MSG (24 per day) and PPS (5-10 per day) and the large positive differences are due to the lower emissivity for PPS. The largest difference occur for North Africa where the PPS broadband emissivity is 0.94 (0.98 over the Atlas mountain range) according to CERES/SARB and 1.00 for MSG leading to 30W/m^2 more SOL for MSG.

ECMWF and RCA have similar SOL bias patterns compared to the CM-SAF data. In the NE part of Europe in winter and over the eastern parts of Europe in spring, RCA overestimate SOL by 20W/m^2 and ECMWF by 10W/m^2. In summer the biases are close to zero or slightly negative over most of Europe for both models. Over North Africa, if we compare the models with MSG-SOL, there is a small overestimate of SOL for ECMWF while RCA is very close to MSG (Fig 20j), while compared to PPS, ECMWF overestimate SOL by up to 30/m^2 and RCA by 20 W/m^2. RCA and ECMWF SOL biases are more similar than what was found for the corresponding SDL biases in the previous section indicating smaller temperature differences between the two models.

In order to see what temperatures the SOL differences corresponds to we have calculated the skin temperature from Eq.2 using the monthly values of SOL and assuming an emissivity of

one everywhere for the models and the CM-SAF products (which we initially thought was the case for both the CM-SAF products). This is not correct since ECMWF, RCA and PPS use different emissivities less than one for land, deserts, canopy and snow (not for PPS) and thereby the calculated temperatures will be colder than the actual skin temperatures. Further, it should have been done on the original SOL temporal resolution and not on the monthly mean values. However, it will give us a hint of the corresponding temperature differences between ECMW and RCA and the GME model.

Figure 12 show the derived T_s from MSG-SOL and the PPS, ECMWF and RCA biases and Figure 21 show the timeseries. Since the emissivity for MSG was assumed to be one MSG T_s (row1, Fig 12) should be close to the GME original T_s, while PPS T_s is smaller as expected e.g. -4K colder over North Africa (row 2, Fig 12). The largest differences between the models and MSG occur for regions with snow or desert, with differences in the calculated T_s of more than +4K in winter and -2K in summer compared to MSG/GME (row 3 and 5, Fig 12). The mean biases are around 1K, except over North Africa where the mean bias is 2.7K for RCA and 4.3K for ECMWF (Table 10). If we use the actual T_s from ECMWF and compare with MSG T_s (Fig 12, row 4) we get an even warmer bias of up to 6K over snow in winter and up to 4K over North Africa. The warm biases would be somewhat reduced if we used the 6 hourly SOL fields instead (since using monthly SOL leads to overestimated MSG/GME T_s due to the quadratic formula in Eq.2).

As mentioned in the previous subsection, ERA40 (ECMWF) might be too warm in winter. Since ERA15 was too cold in winter and too cold over boreal forest in spring and underestimated TET, changes were made in ERA 40, which might have overcompensated the problem according to Kållberg et. al. (1997) and Uppala et. al. (2005). In our comparison, the ECMWF boreal forest area has no bias in spring although the surroundings are much warmer than GME/MSG (e.g. compare March 2006 Fig 12 row 3 and the NE forest area marked in Fig 1). We have compared the two meter temperature (T_{2m}) for ECMWF and RCA with to CRU data for 1985-1989 (not shown) and found that both models have warm biases over NE Europe in winter. The bias is larger for RCA, which partly could be due to the RCA surface scheme calculates T_{2m} over forest regions while the CRU data originates from open land measurements which tend to be colder. We should also remember that ECMWF and RCA have larger cloud cover than CM-SAF over this region and therefore it would be interesting to compare with the cloud cover from the GME model. It is likely that the ECMWF and RCA CFC overestimates are responsible for the higher SDL, lower TET, higher SOL and warmer temperatures we find in the NE of Europe in winter compared to the CM-SAF data, although other factors could contribute.

Finally, in this subsection we have calculated the emissivities for ECMWF and PPS, which are shown in the two last rows in Figure 12. For PPS we used PPS SOL and T_s from MSG/GME and for ECMWF we used its SOL and T_s in Eq.2. We see how the emisssivties varies with regions and seasons with values for ECMWF as low as 0.8 over snow. According to the ECMWF documentation http://www.ecmwf.int/research/ifsdocs/ the window (0.8-12.5μm^{-1}) snow emissivity is 0.93 to 0.98 (depending if the snow is shaded or not) and it is 0.99 outside the window region. The values we get over snow are much lower which could be due to us only using monthly values. The PPS emissivity over NE Europe varies between 0.99 and 1, which is in accordance the value given by CERES/SARB of 0.99 for this region, i.e. our simple derivation appears to give the correct values. GME also has an emissivity of 0.99

over NE Europe and no change if there is snow (personal communication Bodo Ritter, DWD). Even if we do not trust the absolute values for the calculated ECMWF emissivity (Fig 12), the changes over snow for ECMWF might explain part of the large temperature difference between ECMWF and GME.

ECMWF was warmer than MSG over North Africa in our preliminary T_s comparison and also overestimated SOL and TET as previously discussed. This could be due to ECMWF has too high emissivities over North Africa. PPS and RCA (not shown) have lower emissivities than ECMWF over North Africa of about 0.94 and 0.93 compared to the calculated emissivity of 0.98 for ECMWF in Figure 12. GME also have an emissivity of 0.95 over North Africa (personal communication Bodo Ritter, DWD). According to the ECMWF documentation the emissivity for desert in the window region should be 0.93 and 0.99 outside the window region. The broadband emissivity is obtained by convolution of the spectral emissivites. We do not know if the emissivity values in Figure 12 can be trusted due to all the approximations, still the small values over snow and high over desert for ECMWF should be investigated more since they could affect the temperature differences.

To summarize the SOL and T_s comparison, it appears as ECMWF and RCA are much warmer than GME in winter, warmer over North Africa all year and colder in summer over Europe, which we need to investigate further by comparing with independent observations for the time period 2005-2006 and use the actual T_s from all models. For the CM-SAF SOL products we recommend that the same emissivities should be used for MSG and PPS and possibly the same as for GME in order to minimize unnecessary differences and to get the surface budgets correct.

5 Conclusions

We have used CM-SAF cloud and radiation products to evaluate the regional climate model RCA and the ECMWF model over Europe and North Africa. The CM-SAF data has been very useful for this purpose even if some of the products are preliminary such as the cloud water path and the vertically integrated water vapour. The main features in the model and satellite climatologies agree well, although we have identified a number of model biases and satellite problems. The ECMWF mean biases compared to PPS are larger than the CM-SAF target accuracies for most regions, although the correlations are high 0.7 to 0.9 except for cloud water path and water vapour for which the correlations are 0.4. The differences in the cloud and radiation products between the two types of satellites, MSG and PPS, are almost as large as the differences between ECMWF and PPS. RCA has larger biases and standard deviations and worse correlations than ECMWF as expected, since RCA is run without data assimilation. We summarize our findings by geographical area below. (The acronyms for all the CM-SAF products and satellites are given in Appendix 9.1)

- North East Europe in winter

ECMWF and RCA overestimate the cloud fraction by 20% over snow covered regions in NE Europe during winter compared to CM-SAF. For the same region RCA overestimates SDL by

40W/m^2 and ECMWF overestimates SDL by 20W/m^2. The TET bias is close to zero for ECMWF and negative for RCA by up to -40W/m^2. The non-existing bias for ECMWF could possibly be due to a clear-sky overestimate of TET found for ECMWF in other studies (Allen et. al. 2004) cancelling the cloudy sky overestimate. The large surface and TOA long wave biases for RCA might on the other hand have been exaggerated due to extra cooling beneath clouds which has been introduced in the present RCA version.

The excess CFC could also explain the higher SOL 10-30W/m^2 and warmer surface temperatures (4K) found for ECMWF and RCA compared to the GME model, which is used to obtain the CM-SAF SOL products. Differences in snow emissivity for the models might explain part of the temperature differences. However, the RCA and ECMWF overestimate of cloud fraction is believed to be the main reason for the biases.

- North and mid Europe

RCA overestimates TRS by up to 50W/m^2 and underestimates SIS by up to -50W/m^2 in summer and autumn over north and mid Europe. This is most likely due to an overestimation of cloud water by RCA up to 200g/m^2 (i.e. a factor 2-3) compared to PPS. Similar size overestimates of CWP have been found in previous studies (e.g. Lipzig et. al. 2004).

- Mid and south Europe

All year ECMWF underestimates TRS by -14W/m^2 and overestimates SIS in spring-summer by 10W/m^2 and overestimates TET by 14W/m^2 and underestimates SDL -5W/m^2 over mid and south Europe These errors appear to be linked to an underestimation of CFC by 7%. Although, other studies have found that ECMWF underestimates clear-sky TRS because of too low surface albedo (Allen et.al. 2004) and overestimate clear-sky TET, due to lack of cloud ice (Chevallier 2005). We need to evaluate the ECMWF cloudy and clear sky fields separately to help to determine the cause of the biases.

Similar errors occur for RCA in winter-spring, when RCA underestimates CFC by 6% and underestimates TRS by -5W/m^2 and overestimates SIS by 10 W/m^2. The mean RCA biases for TET and SDL are close to zero. This could be due to the changes in the RCA radiation code increasing the long wave cooling beneath clouds which thereby give less bias in TET and SDL despite the underestimation of CFC.

- Sea

The models underestimate cloud fraction over sea by -20% and correspondingly underestimate TRS and SDL and overestimate TET and SIS even more than over land as summarised in the previous bullet. However, since CM-SAF might overestimate the cloud fraction over sea due to problems in the treatment of sub-pixel cloudiness (Johnston and Karlsson 2007), the model radiation errors might be smaller. PPS and especially MSG have excessive cloud amounts over ocean compared to synop as has been found in previous CM-SAF studies. Independent synop and radar/lidar measurements could help in deciding the cloud amount over sea

- Mountains

Mainly RCA but also ECMWF overestimate the cloud fraction at mountain tops by 10-40% and underestimate CFC along mountain ranges by -5 to -20% compared to PPS with somewhat smaller biases compared to MSG. Correspondingly, TRS is overestimated and SIS is underestimated on top of the range. On the leeside, there is an underestimation of TRS and overestimation of SIS. The errors are opposite for long wave fluxes, i.e. too little TET on top and too much along and too much SDL on top and too little SDL along. SOL is overestimated and the surface temperature are much warmer in ECMWF and RCA than in MSG/GME at the mountain tops.

However, the satellites (especially PPS) could be underestimating the cloud fraction for high altitude and snowy regions due to loss of contrast and thereby affecting the surface radiation products since CFC is used in their derivation. Compared to ground based measurements CM-SAF underestimates SDL which is attributed to model altitude and measurements differences (CM-SAF 2007b). Comparing clear and cloudy skies separately and looking at the frequency of cloudiness also for the standard CM-SAF validations would help to clarify if the satellites have problems in these areas and the same should be done for the models.

- North Africa

RCA and ECMWF underestimate TRS (RCA -11W/m^2, ECMWF -28W/m^2) and overestimate TET (RCA 8W/m^2, ECMWF 14W/m^2) and both models overestimate SIS (10W/m^2) and underestimate SDL (5W/m^2) and slightly overestimate CFC (5%) compared to MSG over North Africa. The model and MSG cloud fractions are very similar over North Africa therefore we do not believe the radiation errors are due to cloud fraction errors but could be due to errors in humidity, emissivity or aerosol properties. These TOA errors are similar to what has been found for many other global models (e.g. Allen et. al. 2004) and are attributed to clear sky errors either due to too high surface temperatures, errors in emissivity, albedo or lack of aerosols.

The models and MSG largely underestimates SDL (-40W/m^2) and overestimate SIS (+50W/m^2) compared to PPS. However, we believe these differences are due to the erroneous large PPS cloud fraction (30% more than MSG) which is used for the calculation of the PPS surface fluxes for 2005-2006. This information and any other errors in the CM-SAF cloud fractions that can affect the derived surface radiation fluxes are important to communicate to the users.

6 Future Plans

We would like to extend the model CM-SAF cloud and radiation evaluation to longer time periods to see if the model biases remain using later versions of the CM-SAF data. In order to improve the comparison it would be good if we could match the model and satellite output times. We will derive the model surface radiation, SDL and SIS, in similar ways as CM-SAF to investigate how large difference we get compared with the actual model variables. Some of

the model and satellite differences might be due to the surface and other assumed properties and therefore it would be beneficial to compare emissivities, surface albedo and aerosol climatologies. We also plan to do sensitivity tests changing the model cloud and radiation parameterisations, to explore the impact on the model climate.

We hope there will be new CM-SAF products that could help in the model evaluation and development. For example a separation into clear and cloud sky radiation fluxes would help us to better identify model and satellite errors. It would also be good to extend the comparison beyond monthly means, to look at the diurnal cycle, histograms and variability for the satellites and models cloud and radiation fields. In the evaluation of the CM-SAF data against other observations we recommend to single out deserts, mountain and snowy regions, areas that have stood out in this comparison.

7 Acknowledgements

The study has been funded by EUMETSAT as part of the CM-SAF Visiting Scientist program. I would like to thank Britta Thies and Diana Stein for all help retrieving the CM-SAF data and Karl-Göran Karlsson for valuable comments to the manuscript and many others from the CM-SAF group for answering questions and giving support. Finally, many thanks to Anneli Arkler for making this report printable.

8 References

Allan, R. P., M. A. Ringer, and A. Slingo 2003. Evaluation of moisture in the Hadley Centre Climate Model using simulations of HIRS water vapour channel radiances, Quarterly Journal of Royal Met. Soc., 129, 3371-3389.

Allan, R. P., M. A. Ringer, J. A. Pamment and A. Slingo 2004. Simulation of the Earth's radiation budget by the European Centre for Medium Range Weather Forecasts 40-year Reanalysis (ERA40) J. Geophys. Res., 109, D18107, doi:10.1029/2004JD004816.

Allan, R. P. 2007a. Improved simulation of water vapour and clear-sky radiation using 24 hour forecasts from ERA40, Tellus, 59A, 336-343. PDF (DOI: 10.1111/j.1600-0870.2007.00229.x)

Allan, R. P., A. Slingo, S.F. Milton and M.A. Brooks 2007b. Evaluation of the Met Office global forecast model using Geostationary Earth Radition Budget (GERB) data, Q. J. Roy. Meteorol. Soc., 133, 1993-2010

Chevallier, F., G. Kelly, A.J. Simmons, S. Uppala, and A. Hernandez, 2005. High Clouds over Oceans in the ECMWF 15- and 45-Yr Reanalyses. J. Climate, 18, 2647–2661.

CM-SAF 2007a. http://www.dwd.de/en/FundE/Klima/KLIS/int/CM-SAF/index.htm or

http://orias.dwd.de/safira/action/viewHome

CM-SAF 2007b. CM-SAF User Manual – Products. Doc.No: SAF/CM/DWD/UMP/1

CM-SAF 2007c. CM-SAF Scientific Report Validation of the TOA radiative fluxes Version 120 products. Doc. No.:SAF/CM/SR/SFCFLX/2

CM-SAF 2005 Products Validation Report Summary Doc.No: SAF/CM/DWD/PVRS/1

Davies, H. C., 1976. A lateral boundary formulation for multi-level prediction models. Quart. J. Roy. Meteor. Soc., 102, 405-418.

Fouquart, Y. and Bonnel, B., 1980. Computations of solar heating of the earth's atmosphere: A new parameterization. Beitr. Phys. Atmos., 53, 35-62.

Georgelin, M. and co-authors 2000. The second COMPARE exercise: A model intercomparison using a case of a typical mesoscale orographic flow, the PYREX IOP3. Quarterly Journal of the Royal Meteorologica l Society, 126, pp 991-1030.

Gupta, S. K., 1989. A parameterization for longwave surface radiation from Sun-synchronous satellite data. J. Climate, 2:305-320.

Gupta, S. K., W. L. Darnell, and A. C. Wilber, 1992. A parameterization for longwave surface radiation from satellite data: Recent improvements, J. Appl. Meteorol., 31, 1361.

Iacono, M.J., E.J. Mlawer, S.A. Clough, and J.-J. Morcrette, 2000. Impact of an improved longwave radiation model, RRTM, on the energy budget and thermodynamic properties of the NCAR community climate model, CCM3, J. Geophys. Res., 105, 14873-14890.

Illingworth, A.J., R.J. Hogan, E.J. O'Connor, D. Bouniol, M.E. Brooks, J. Delanoë, D.P. Donovan, J.D. Eastment, N. Gaussiat, J.W.F. Goddard, M. Haeffelin, H.K.

Baltink, O.A. Krasnov, J. Pelon, J.M. Piriou, A. Protat, H.W.J. Russchenberg, A. Seifert, A.M. Tompkins, G.J. van Zadelhoff, F. Vinit, U. Willén, D.R. Wilson, and C.L. Wrench, 2007. Cloudnet. Bull. Amer. Meteor. Soc., 88, 883–898.

Johnston, S. and K-G. Karlsson, 2007. METEOSAT-8 SEVIRI and NOAA AVHRR cloud products - A Climate Monitoring SAF comparison study. SMHI Reports Meteorology, No. 127. 41 pp.

Jones CG, Willén U, Ullerstig A, Hansson U 2004. The Rossby Centre Regional Atmospheric Climate Model Part I: Model Climatology and Performance for the Present Climate over Europe. AMBIO: A Journal of the Human Environment: Vol. 33, No. 4 pp. 199–210

Kain, J.S., and J.M. Fritsch, 1993. Convective parameterization for mesoscale models: The Kain- Fritsch scheme. In: The representation of cumulus convection in numerical models. Meteor. Monogr., No. 24, Amer. Meteor. Soc., 165-170.

Karlsson, K., U. Willén, C. Jones, and K. Wyser 2008. Evaluation of regional cloud climate simulations over Scandinavia using a 10-year NOAA Advanced Very High Resolution Radiometer cloud climatology, J. Geophys. Res., 113, D01203, doi:10.1029/2007JD008658.

Kjellström, E., Bärring, L., Gollvik, S., Hansson, U., Jones, C., Samuelsson, P., Rummukainen, M., Ullerstig, A., Willén U. and Wyser, K., 2005. A 140-year simulation of European climate with the new version of the Rossby Centre regional atmospheric climate model (RCA3). Reports Meteorology and Climatology 108, SMHI, SE-60176 Norrköping, Sweden, 54 pp.

Kållberg, P., 1997 Aspects of the reanalysed climate. ECMWF Reanalysis Proj. Rep.2, 89 pp.

Majewski, D., D. Liermann, P. Prohl, B. Ritter, M. Buchhold, T. Hanisch, G. Paul, W. Wergen, and J. Baumgardner, 2002: The Operational Global Icosahedral–Hexagonal Gridpoint Model GME: Description and High-Resolution Tests. Mon. Wea. Rev., 130, 319–338

Mitchell, T.D and P.D. Jones, 2005. An improved method of constructing a database of monthly climate observations and associated high-resolution grids. Int. J.Clim. vol 25,DOI:10.1002/joc.1181 693 – 712.

Mlawer, E.J., Taudman, S.J. Brown, P.D., Iacono M.J., and S.A. Clough, 1997. Radiative transfer for inhomogeneous atmosphere: RRTM, a validated correlated-k model for the longwave. J. Geophys. Res. 102 D14, pp. 16663–16682.

Morcrette J.-J. 2002. The Surface Downward Longwave Radiation in the ECMWF Forecast System. J. Climate, 15, 1875-1892.

Rasch, P.J. and J.E. Kristjansson, 1998: A comparison of the CCM3 model climate using diagnosed and predicted condensate parameterisations, J. Climate, 11, 1587-1614.

Räisänen, P., M. Rummukainen, J. Räisänen, 2000. Modification of the HIRLAM Radiation scheme for use in the Rossby Centre Regional Atmospheric Climate model., University of Helsinki Reports, 49, 71pp.

Roebeling, R.A., H.M. Deneke and A.J. Feijt, 2007. Validation cloud liquid water path retrievals from SEVIRI using one year of CLOUDNET observations. Submitted to J. Appl. Meteo.

Rummukainen, M., Räisänen, J., Bringfelt, B., Ullerstig, A., Omstedt, A., Willén, U., Hansson, U. and Jones, C. 2001. A regional climate model for northern Europe: model description and results from the downscaling of two GCM control simulations. Clim. Dyn. 17, 339-359.

Sass, B. H., L. Rontu, P. Räisänen, 1994. HIRLAM-2 Radiation scheme: Documentation and Tests. The Hirlam 3 Project, c/o SMHI , Technical Report 16, 43pp

Savijärvi H., 1990. Fast radiation parametrization schemes for mesoscale and short-range forecast models. J. Appl. Meteor. , 29, 437-447

Schröder, M., van Lipzig, N., Ament, F., Chaboureau, J-P., Crewell, S., Fischer, J., Matthias, V., van Meijgaard, E., Walther, A., Willén, U. 2006. Comparison of model predicted low-level cloud parameters with satellite remote sensing observations during the BALTEX Bridge Campaigns. Atmos. Res. doi:10.1016/j.atmosres.2005.12.005

Simmons A.J. (Ed) 2001. Workshop in reanalysis. ECMWF Rep.Ser. 3, 443p. ECMWF, Reading, UK.

Slingo J.M., 1987. The development and verification of a cloud prediction scheme for the ECMWF model. Q.J.R. Meteorol. Soc. 113, 899-928.

Slingo, A. 1989, A GCM parameterization for the shortwave radiative properties of water clouds, J. Atmos. Sci. 46 (1989), pp. 1419–1427.

Tiedtke, M., 1989. A comprehensive mass flux scheme for cumulus parameterization in large-scale models. Mon. Weather Rev., 117, 1779-1800.

Tiedtke, M., 1993. Representation of clouds in large-scale models. Mon. Weather Rev., 121, 3040-3061

Undén P. and co-authors, 2002. HIRLAM-5 Scientific Documentation, HIRLAM-5 project, (Available from SMHI, c/o Per Undén, S-601 76 Norrköping, Sweden, or from hirlam.knmi.nl under Publications/Scientific doc

Uppala, S. M., P.W. Kallberg, A.J. Simmons, U. Andrae, V. da Costa Bechtold, M. Fiorino, J.K Gibson, J. Haseler, A. Hernandez, G.A. Kelly, X. Li, K. Onogi, S. Saarinen, N. Sokka, R.P. Allan, E. Andersson, K. Arpe, M.A. Balmaseda, A.C.M. Beljaars, L. van de Berg, J. Bidlot, N. Bormann, S. Caires, F. Chevallier, A. Dethof, M. Dragosavac, M. Fisher, M. Fuentes, S. Hagemann, E. Holm, B.J. Hoskins, L. Isaksen, P.A.E.M. Janssen, R. Jenne, A.P. McNally, J.-F. Mahfouf, J.-J. Morcrette, N.A Rayner, R.W. Saunders, P. Simon, A. Sterl, K.E. Trenberth, A. Untch, D. Vasiljevic, P. Viterbo and J. Woollen 2005. The ERA-40 Re-analysis, Q. J. Roy. Meteorol. Soc., 131, 2961-3012.

van Lipzig, N., Schröder, M., Crewell, S., Ament, F., Chaboureau, J-P., Löhnert, U., Matthias, V., van Meijgaard, E., Quante, M., Willén, U., Yen, W., 2006. Model predicted low-level cloud parameters: Part I: Comparison with observations from the BALTEX Bridge Campaigns. Atmos. Res.doi:10.1016/j.atmosres.2006.01.010

Yang, S.K., Y.T. Hou, A.J. Miller, and K.A. Campana, 1999. Evaluation of the Earth Radiation Budget in NCEP–NCAR Reanalysis with ERBE. J. Climate, 12, 477–493.

9 Appendix

9.1 Acronyms

CFC	Fractional Cloud Cover
CWP	Cloud Water Path, vertically integrated cloud water
HTW	Vertically Integrated water vapour
TRS	Top of the atmosphere Reflected Solar radiation
TET	Top of the atmosphere Emitted Thermal radiation
SIS	Surface Incoming Solar radiation
SDL	Surface Downwelling Longwave radiation
SOL	Surface Outgoing Longwave radiation
EUMETSAT	EUropean organisation for the exploitation of METeorological SATellites
CM-SAF	Satellite Application Facility on Climate Monitoring
PPS	Polar Platform System (polar orbiting satellites)
MSG	Meteosat Second Generation (geostationary satellites)

9.2 Tables

Description	From	To	Filename	Order Id
130 **CFC PPS**	01.01.2005	01.03.2005	CFCmm2005010100001300700101 01CA.hdf	484
140 **CFC PPS**	01.04.2005	01.07.2005	CFCmm2005040100001400700101 01CA.hdf	390
150 **CFC PPS**	01.08.2005	01.12.2006	CFCmm2005080100001500700101 01CA.hdf	400, 611
210 **CFC MSG**	01.09.2005	01.12.2006	CFCmm2005090100002100700160 01CA.hdf	384, 612
130 **CWP PPS**	01.01.2005	01.03.2005	CWPmm2005010100001300700107 01CA.hdf	485
140 **CWP PPS**	01.04.2005	01.07.2005	CWPmm2005040100001400700107 01CA.hdf	392
150 **CWP PPS**	01.08.2005	01.12.2006	CWPmm2005080100001500700107 01CA.hdf	402, 621
210 **CWP MSG**	01.09.2005	01.12.2006	CWPmm2005090100002100700165 01CA.hdf	403, 622
210 **HTW PPS** from ATOVS	01.09.2005	01.08.2006	HTWmm2005090100002100800173 01CA.hdf	474
210 **HTW MSG** from SEVIRI	01.09.2005	01.08.2006	HTWmm2005090100002100700170 01CA.hdf	283 473, 619
100 **TRS MSG**	01.01.2005	01.12.2005	TRSmm2005010100001000200116 01CD.hdf	458
120 **TRS MSG**	01.01.2006	01.12.2006	TRSmm2006010100001200200116 01CD.hdf	610
100 **TET MSG**	01.01.2005	01.12.2005	TETmm2005010100001000200117 01CD.hdf	476
120 **TET MSG**	01.01.2006	01.12.2006	TETmm2006010100001200200117 01CD.hdf	608
100 **TIS MSG**	01.01.2005	01.12.2005	TISmm2005010100001000200115 01CD.hdf	456
120 **TIS MSG**	01.01.2006	01.12.2006	TISmm2006010100001200200115 01CD.hdf	609
130 **SIS PPS**	01.01.2005	01.03.2005	SISmm2005010100001300700108 01CA.hdf	483
140 **SIS PPS**	01.04.2005	01.07.2005	SISmm2005040100001400700108 01CA.hdf	407
150 **SIS PPS**	01.08.2005	01.12.2006	SISmm2005080100001500700108 01CA.hdf	408, 614
210 **SIS MSG**	01.09.2005	01.12.2006	SISmm2005090100002100700179 01CA.hd	410, 625
130 **SDL PPS**	01.01.2005	01.03.2005	SDLmm2005010100001300700112 01CA.hdf	452
140 **SDL PPS**	01.04.2005	01.07.2005	SDLmm2005040100001400700112 01CA.hdf	284
150 **SDL PPS**	01.08.2005	01.12.2006	SDLmm2005080100001500700112 01CA.hdf	398, 613
210 **SDL MSG**	01.09.2005	01.12.2006	SDLmm2005090100002100700178 01CA.hdf	388, 623
130 **SOL PPS**	01.01.2005	01.03.2005	SOLmm2005010100001300700111 01CA.hdf	489
140 **SOL PPS**	01.04.2005	01.07.2005	SOLmm2005040100001400700111 01CA.hdf	416
150 **SOL PPS**	01.08.2005	01.12.2006	SOLmm2005080100001500700111 01CA.hdf	444, 615
210 **SOL MSG**	01.09.2005	01.12.2006	SOLmm2005090100002100700180 01CA.hdf	445, 627

Table 1. List of CM-SAF data sets used in this study for the time period 2005-2006.

Mean CFC	Land1	Land2	Land3	Sea1	Sea2
PPS	66.9	56.6	51.6	82.8	49.4
RCA	67.9	50.8	25.4	66.4	31.8
ECMWF	68.7	49.3	25.9	70.9	32.3
RCA compared to PPS					
Bias	1.0	-5.8	**-26.2**	**-16.3**	**-17.6**
Standard dev	13.0	13.2	16.6	9.4	9.4
Correlation	0.24	0.55	0.33	0.58	0.63
ECMWF compared to PPS					
Bias	1.5	-6.7	**-25.3**	**-11.7**	**-16.6**
Standard dev	10.3	9.8	15.5	6.9	7.2
Correlation	0.42	0.71	0.31	0.73	0.77
RCA compared to ECMWF					
Bias	-0.9	1.0	-0.8	-4.6	-1.0
Standard dev	11.8	10.2	7.9	10.0	8.0
Correlation	0.36	0.74	0.80	0.52	0.69

Table 2. The CFC statistics for 2005-2006. The first part show the mean CFC values, the second part the difference statistics for RCA compared to PPS, the third ECMWF compared to PPS and the fourth RCA compared to ECMWF. The target accuracy for CM-SAF CFC is 10%, any bias exceeding this value is shown in red (positive) or blue (negative). All the numbers are in % except the correlation.

Mean CWP	Land1	Land2	Land3	Sea1	Sea2
PPS	79.3	71.5	24.7	64.8	43.5
RCA	235.5	165.8	44.9	248.4	71.8
ECMWF	79.9	56.4	16.9	90.9	31.9
RCA compared to PPS					
Bias	**156.1**	**94.4**	**20.1**	**183.5**	**28.4**
Standard dev	91.6	84.9	29.6	77.0	38.2
Correlation	0.27	0.37	0.38	0.36	0.35
ECMWF compared to PPS					
Bias	1.1	**-14.7**	-7.6	**26.1**	**-11.3**
Standard dev	51.4	35.2	14.3	32.6	22.7
Correlation	0.37	0.55	0.48	0.42	0.45
RCA compared to ECMWF					
Bias	**161.1**	**110.4**	**26.5**	**159.6**	**39.0**
Standard dev	62.7	68.2	22.7	59.7	22.7
Correlation	0.60	0.67	0.75	0.81	0.70

Table 3. The CWP statistics for 2005-2006. The target accuracy for CM-SAF CWP is 15%, any bias exceeding this value is shown in red (positive) or blue (negative). All numbers are in g/m^2 except the correlation. The table division is as in Table 2.

Mean HTW	Land1	Land2	Land3	Sea1	Sea2
PPS	12.9	16.9	20.0	13.2	18.0
RCA	12.6	15.8	16.6	14.8	19.0
ECMWF	12.9	16.6	17.1	14.9	20.2
RCA compared to PPS					
Bias	-0.3	-1.2	**-3.4**	1.5	1.0
Standard dev	1.1	2.4	2.9	1.0	1.7
Correlation	0.85	0.40	0.07	0.95	0.55
ECMWF compared to PPS					
Bias	-0.6	-1.1	**-3.5**	1.3	1.5
Standard dev	1.0	2.5	3.2	0.9	1.7
Correlation	0.85	0.45	0.01	0.96	0.62
RCA compared to ECMWF					
Bias	0.2	-0.2	-0.1	0.3	-0.6
Standard dev	0.7	1.1	1.0	0.6	1.2
Correlation	0.95	0.91	0.93	0.97	0.84

Table 4. The HTW statistics for 2005-2006. The target accuracy for CM-SAF HTW is 1.5 kg/m^2, any bias exceeding this value is shown in red (positive) or blue (negative). All numbers are in kg/m^2 except the correlation. The table division is as in Table 2.

Mean TRS	Land1	Land2	Land3	Sea1	Sea2
PPS	90.7	100.9	117.7	90.1	69.6
RCA	95.8	110.8	106.2	95.0	75.0
ECMWF	89.3	92.8	93.1	83.6	60.0
RCA compared to MSG					
Bias	5.1	9.9	**-11.4**	4.9	5.4
Standard dev	11.4	11.8	17.6	13.2	10.2
Correlation	0.73	0.79	0.67	0.76	0.55
ECMWF compared to MSG					
Bias	**-11.8**	**-14.0**	**-28.2**	**-15.7**	**-10.6**
Standard dev	8.5	9.5	14.8	9.0	7.4
Correlation	0.87	0.87	0.85	0.88	0.80
RCA compared to ECMWF					
Bias	**18.5**	**25.8**	**16.4**	**22.3**	**16.2**
Standard dev	11.8	11.9	11.5	11.1	7.8
Correlation	0.74	0.82	0.66	0.85	0.64

Table 5. The TRS statistics for 2005-2006. The target accuracy for CM-SAF TRS is 10 W/m^2, any bias exceeding this value is shown in red (positive) or blue (negative). All numbers are in W/m^2 except the correlation. The table division is as in Table 2.

Mean TET	Land1	Land2	Land3	Sea1	Sea2
PPS	212.6	228.9	261.0	217.9	252.7
RCA	202.0	228.4	268.5	216.2	260.6
ECMWF	226.6	244.7	278.3	233.8	269.2
RCA compared to MSG					
Bias	**-10.6**	-0.5	7.5	-1.7	7.8
Standard dev	9.8	10.1	9.2	8.2	5.8
Correlation	0.60	0.83	0.87	0.80	0.89
ECMWF compared to MSG					
Bias	**11.0**	**14.4**	**14.4**	**14.0**	**15.2**
Standard dev	3.6	4.4	4.2	3.2	3.5
Correlation	0.86	0.94	0.93	0.95	0.97
RCA compared to ECMWF					
Bias	**-21.7**	**-14.6**	-6.9	**-16.0**	-6.7
Standard dev	9.5	10.4	9.2	7.2	6.0
Correlation	0.64	0.85	0.93	0.84	0.91

Table 6. The TET statistics for 2005-2006. The target accuracy for CM-SAF TET is 10 W/m^2, any bias exceeding this value is shown in red (positive) or blue (negative). All numbers are in W/m^2 except the correlation. The table division is as in Table 2.

Mean SIS	Land1	Land2	Land3	Sea1	Sea2
PPS	120.8	167.6	237.5	124.5	240.5
RCA	107.5	166.7	270.7	103.6	241.0
ECMWF	142.5	197.8	276.6	146.4	264.1
RCA compared to PPS					
Bias	**-13.3**	-0.9	**33.1**	**-20.9**	0.5
Standard dev	13.8	16.6	22.9	12.9	12.8
Correlation	0.68	0.84	-0.19	0.87	0.64
ECMWF compared to PPS					
Bias	-0.5	5.3	**32.9**	0.6	4.6
Standard dev	10.0	11.4	21.8	8.9	11.2
Correlation	0.81	0.92	-0.09	0.95	0.76
RCA compared to ECMWF					
Bias	**-13.2**	-5.4	1.9	**-23.5**	-3.1
Standard dev	14.3	16.3	6.6	13.7	10.2
Correlation	0.69	0.89	0.71	0.89	0.77

Table 7. The SIS statistics for 2005-2006. The target accuracy for CM-SAF SIS is 10 W/m^2, any bias exceeding this value is shown in red (positive) or blue (negative). All numbers are in W/m^2 except the correlation. The table division is as in Table 2.

Mean SDL	Land1	Land2	Land3	Sea1	Sea2
PPS	285.1	310.7	343.9	319.2	346.5
RCA	296.3	312.6	328.6	318.0	334.9
ECMWF	286.5	307.3	327.6	308.4	333.0
RCA compared to PPS					
Bias	**11.1**	1.8	**-15.3**	-1.2	**-11.6**
Standard dev	12.8	13.0	17.6	9.4	7.9
Correlation	0.73	0.73	0.70	0.89	0.70
ECMWF compared to PPS					
Bias	-1.0	-5.1	**-19.3**	**-10.9**	**-13.4**
Standard dev	8.7	9.3	16.9	6.2	5.8
Correlation	0.86	0.87	0.76	0.94	0.76
RCA compared to ECMWF					
Bias	**10.8**	7.1	3.0	9.8	1.6
Standard dev	9.6	9.4	7.3	7.7	6.5
Correlation	0.81	0.79	0.85	0.93	0.74

Table 8. The SDL statistics for 2005-2006. The target accuracy for CM-SAF SDL is 10 W/m^2, any bias exceeding this value is shown in red (positive) or blue (negative). All numbers are in W/m^2 except the correlation. The table division is as in Table 2.

Mean SOL	Land1	Land2	Land3	Sea1	Sea2
PPS	331.1	365.7	402.0	363.5	414.6
RCA	337.8	370.6	417.0	364.2	414.7
ECMWF	339.0	373.9	431.7	365.0	416.8
RCA compared to PPS					
Bias	6.6	5.0	**15.0**	0.7	0.2
Standard dev	8.9	9.6	9.7	3.4	5.1
Correlation	0.91	0.92	0.87	0.98	0.91
ECMWF compared to PPS					
Bias	4.1	5.0	**24.8**	2.0	2.6
Standard dev	7.3	8.4	12.9	2.3	3.1
Correlation	0.93	0.92	0.80	0.99	0.96
RCA compared to ECMWF					
Bias	2.0	0.2	-9.5	-1.1	-1.9
Standard dev	6.1	7.3	9.2	2.4	3.7
Correlation	0.94	0.94	0.90	0.99	0.95

Table 9. The SOL statistics for 2005-2006. The target accuracy for CM-SAF SOL is 10 W/m^2, any bias exceeding this value is shown in red (positive) or blue (negative). All numbers are in W/m^2 except the correlation. The table division is as in Table 2.

Mean T_s	Land1	Land2	Land3	Sea1	Sea2
PPS	2.7	9.8	16.6	9.7	19.1
RCA	4.2	10.8	19.3	9.8	19.2
ECMWF	4.5	11.4	21.8	10.0	19.5
RCA compared to PPS					
Bias	1.5	1.0	**2.7**	0.1	0.0
Standard dev	1.9	1.9	1.7	0.7	0.9
Correlation	0.91	0.92	0.87	0.98	0.91
ECMWF compared to PPS					
Bias	1.0	1.0	**4.3**	0.4	0.4
Standard dev	1.6	1.6	2.2	0.5	0.6
Correlation	0.93	0.92	0.80	0.99	0.96
RCA compared to ECMWF					
Bias	0.4	0.0	-1.6	-0.2	-0.3
Standard dev	1.3	1.4	1.6	0.6	0.7
Correlation	0.94	0.93	0.90	0.99	0.95

Table 10. The T_s statistics for 2005-2006. The target accuracy for CM-SAF SOL of 10 W/m^2 corresponds to an accuracy of 2°C for T_s, any bias exceeding this value is shown in red (positive) or blue (negative). All numbers are in °C except the correlation. The table division is as in Table 2.

9.3 Figures

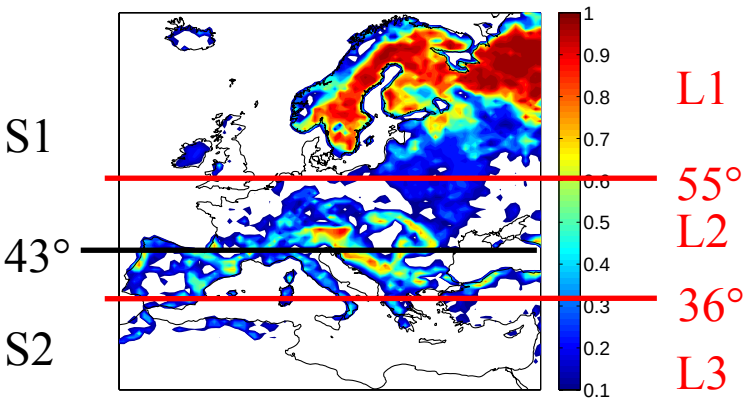

Figure 1. The fraction of forest in RCA. The red lines mark the three land regions; land points north of 55°N (North Europe: L1), land points between 36°N and 55°N (middle Europe: L2), land south of 36°N (North Africa: L3), and the black line; sea points north of 43°N (the Atlantic: S1) and sea points south of 43°N (the Mediterranean Sea=S2).

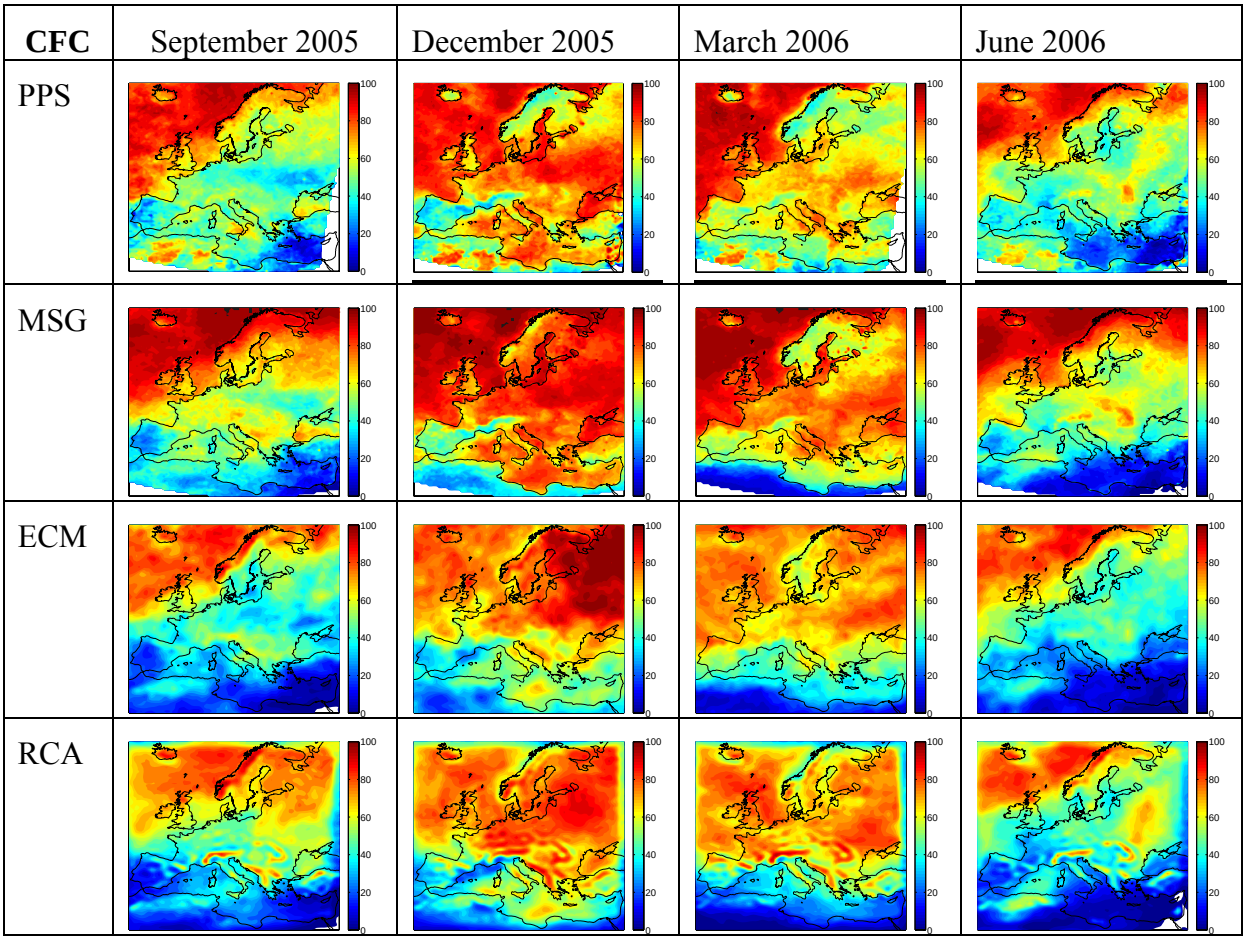

Figure 2. The Cloud fraction (%) in row 1) PPS 2) MSG 3) ECMWF and 4) RCA for September, December 2005 and March, June 2006.

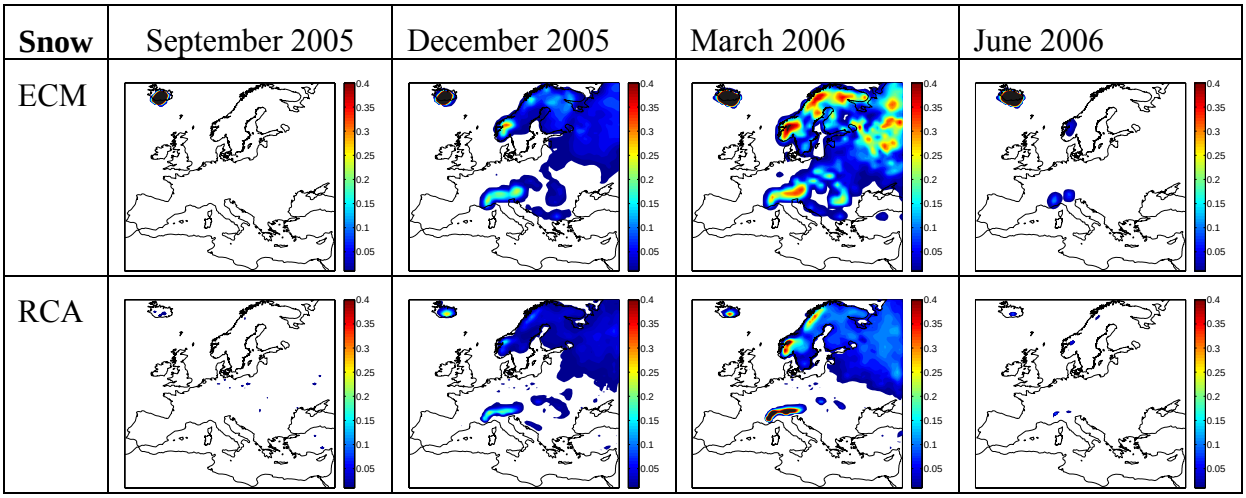

Figure 3. The Snow water equivalent (m), in row 1) for ECMWF and 2) RCA for September, December 2005 and March, June 2006.

CFC Bias	September 2005	December 2005	March 2006	June 2006
MSG-PPS	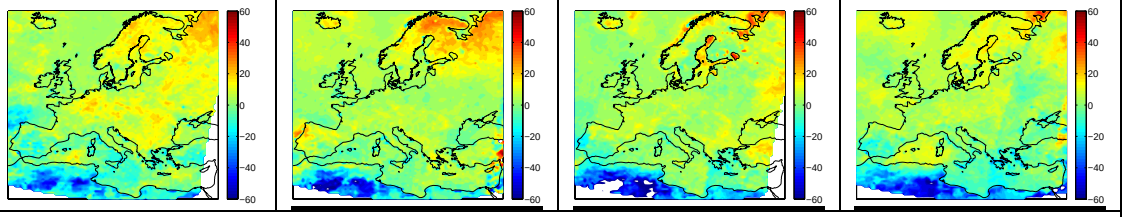			
ECM-PPS	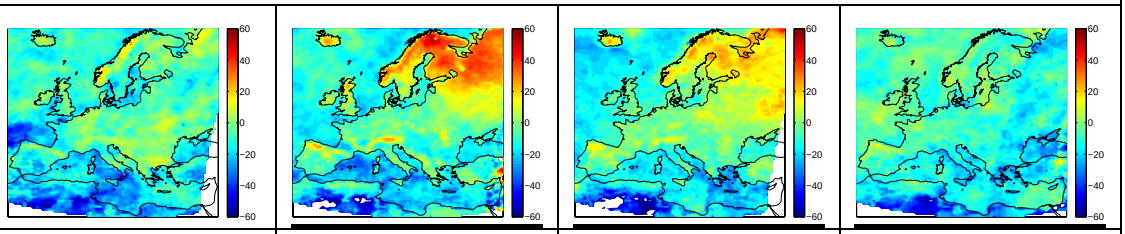			
ECM-MSG	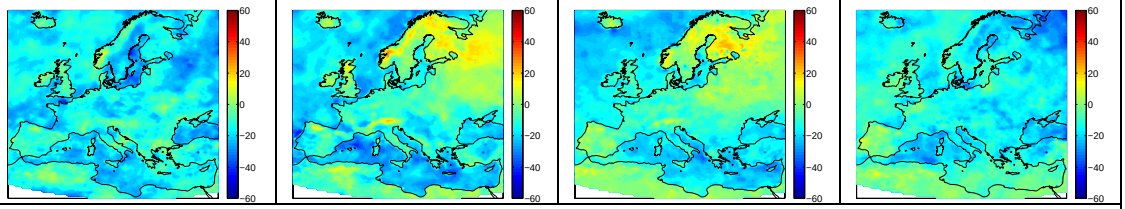			
RCA-PPS	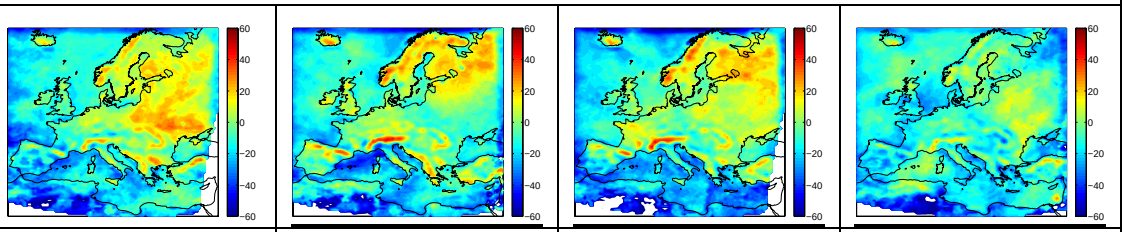			
RCA-MSG	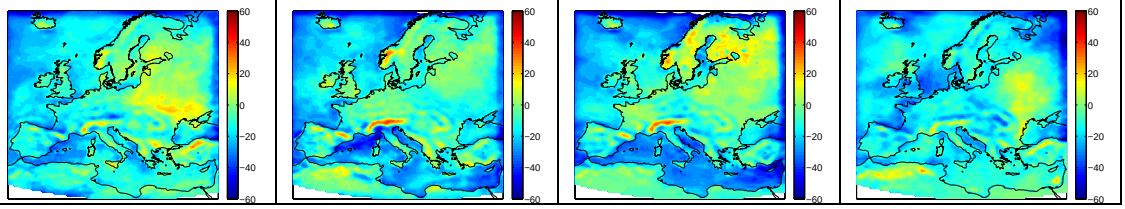			

Figure 4. The difference in cloud fraction (%), in row 1) MSG-PPS 2) ECMWF-PPS 3) ECMWF-MSG 4) RCA-PPS and 5) RCA-MSG for September, December 2005 and March, June 2006.

CWP	September 2005	December 2005	March 2006	June 2006
PPS	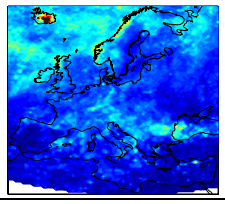	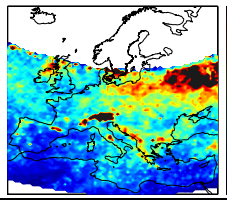	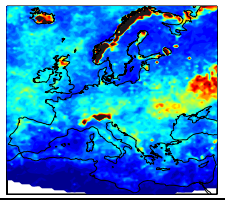	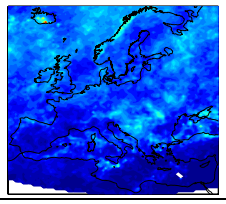
MSG-PPS	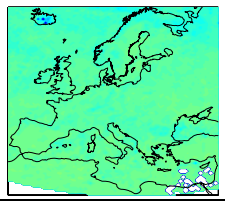	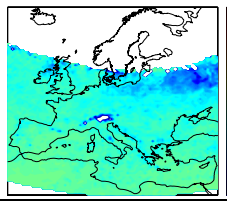	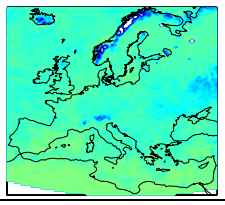	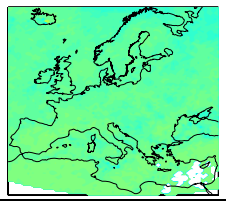
ECM-PPS	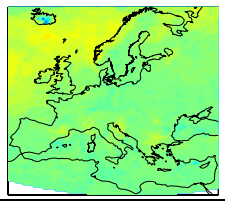	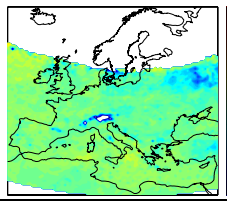	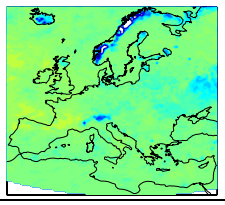	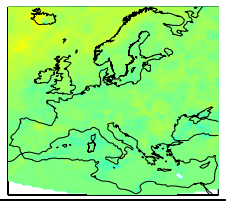
RCA-PPS	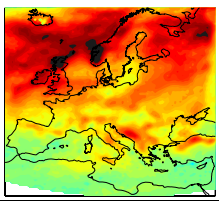	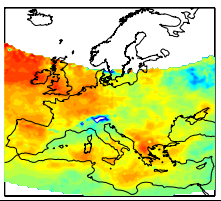	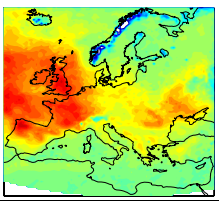	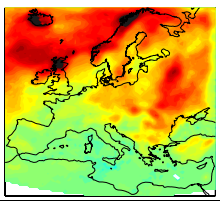

Figure 5. The Cloud Water Path (kg/m^2) for 1) PPS and the differences 2) MSG-PPS 3)ECMWF-PPS, 4) RCA-PPS for September, December 2005 and March, June 2006.

HTW	September 2005	December 2005	March 2006	June 2006
PPS	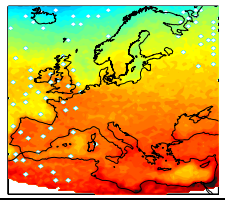	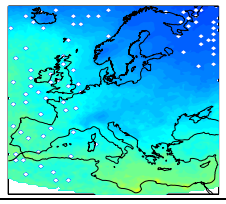	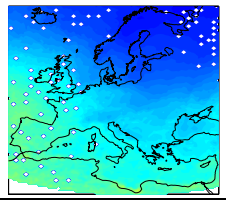	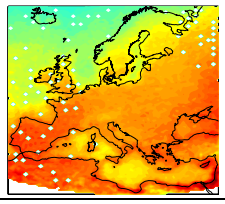
MSG-PPS	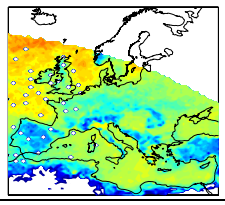	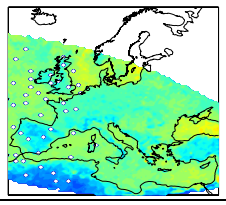	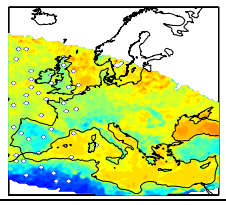	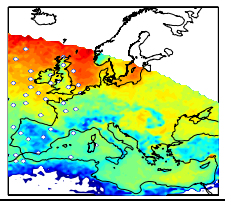
ECM-PPS	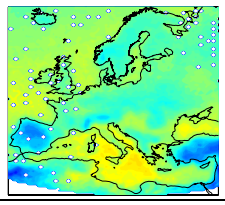	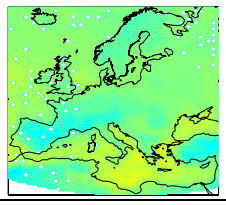	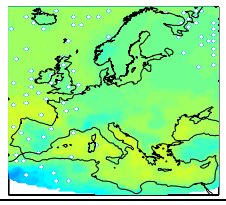	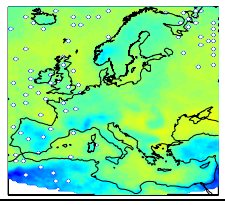
RCA-PPS	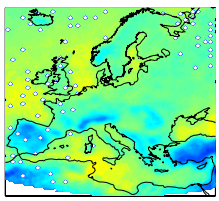	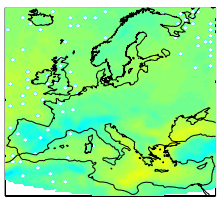	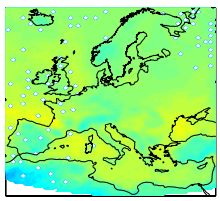	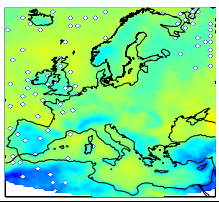

Figure 6. The vertically Integrated Water Vapour (kg/m^2) for 1) PPS/ATOVS and the differences 2) MSG-PPS 3) ECMWF-PPS 4) RCA-PPS for September, December 2005 and March, June 2006.

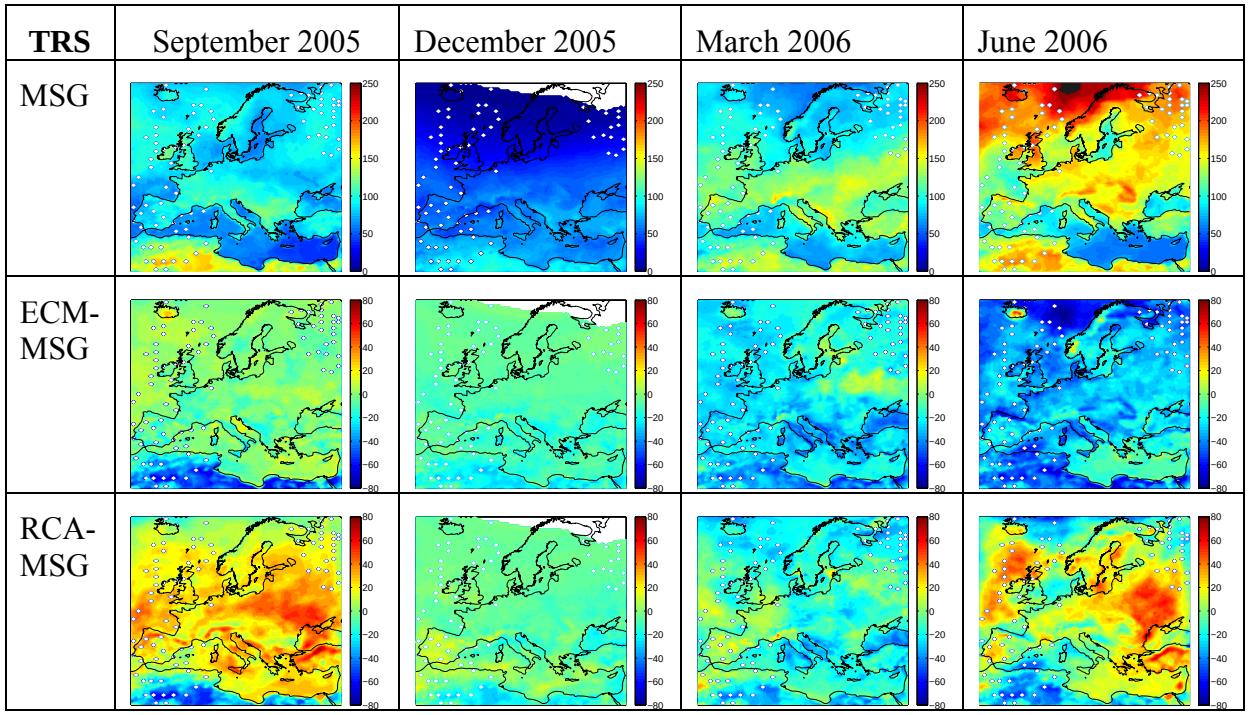

Figure 7. The Reflected Solar radiative flux (W/m^2) at the Top of the Atmosphere for 1) MSG and Aqua/Terra and the differences 2) ECMWF-MSG 3) RCA-MSG for September, December 2005 and March, June 2006.

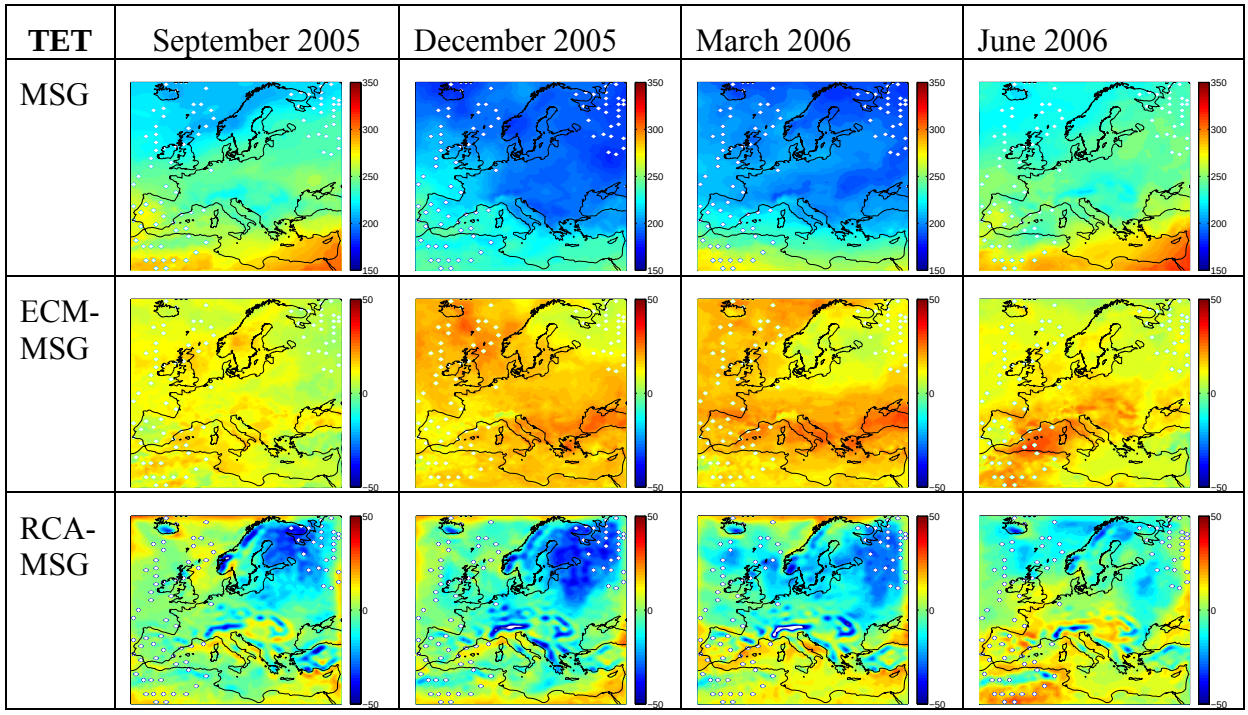

Figure 8. The Emitted Thermal radiative flux (W/m^2) at the Top of the Atmosphere for 1) MSG and Aqua/Terra and the differences 2) ECMWF-MSG 3) RCA-MSG for September, December 2005 and March, June 2006.

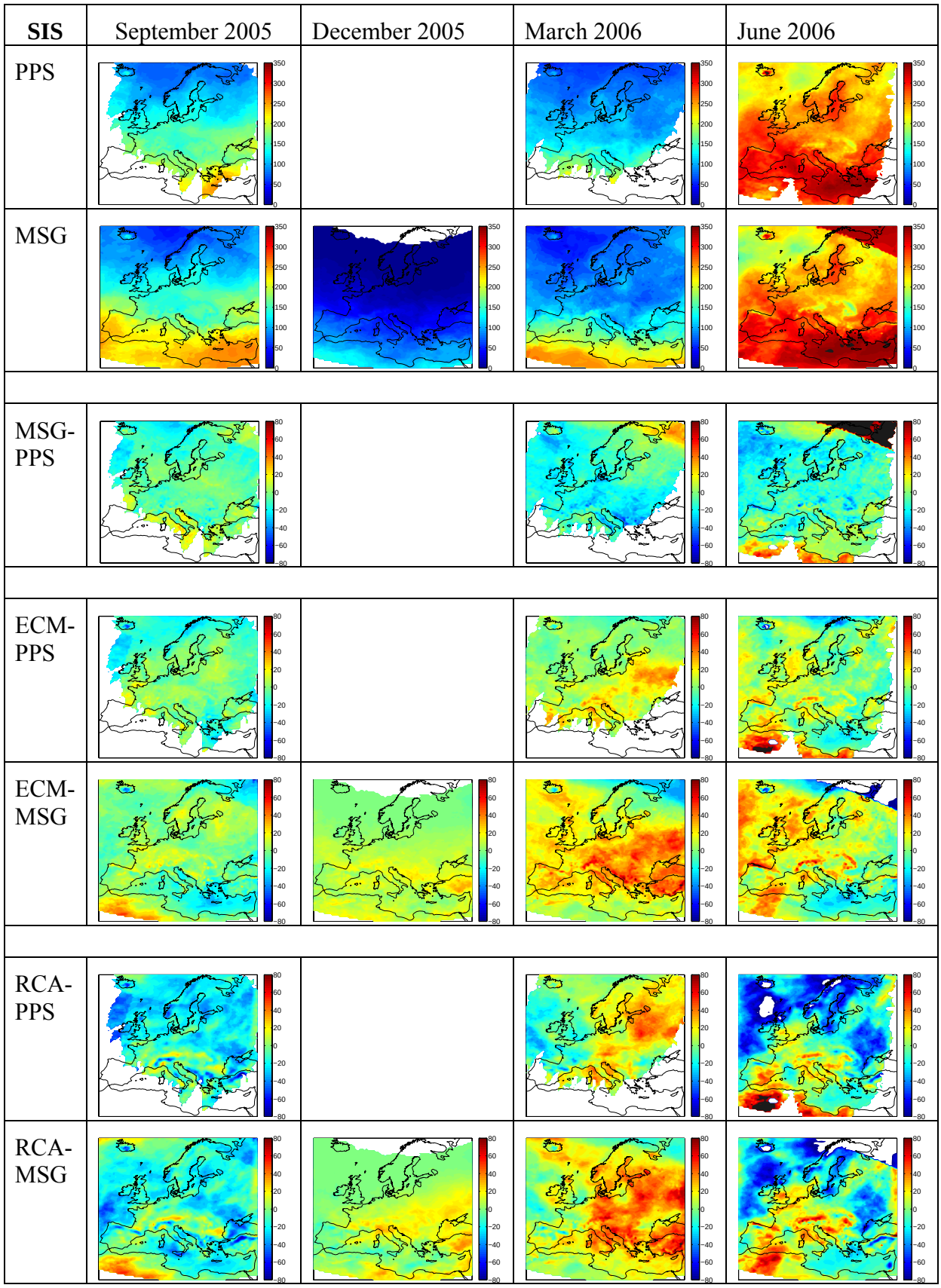

Figure 9. The surface incoming shortwave radiation (W/m^2) for 1) PPS and the differences 2) MSG-PPS 3) ECMWF-PPS 4) ECMWF-MSG 5) RCA-PPS 6) RCA-MSG for September, December 2005 and March, June 2006.

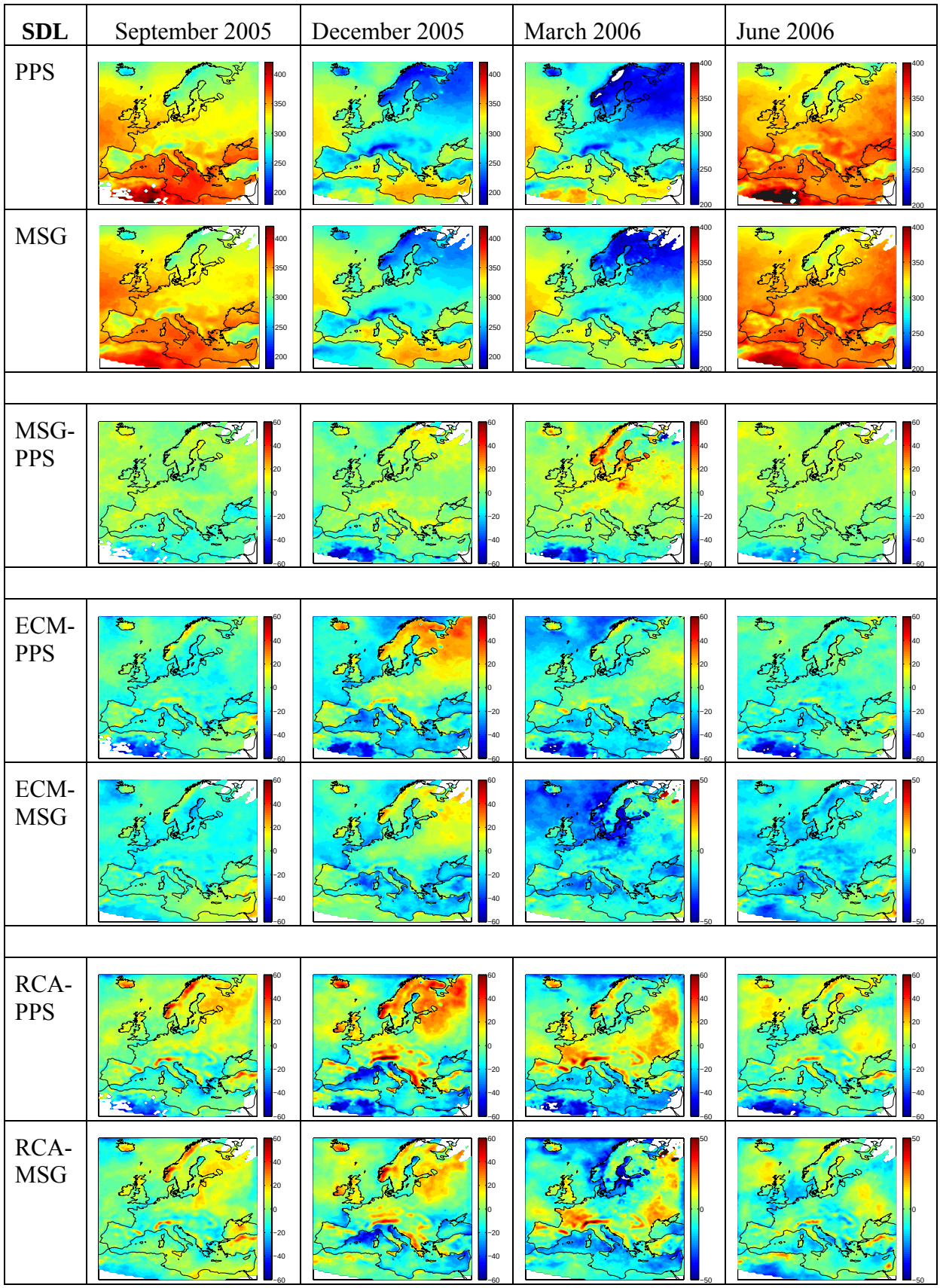

Figure 10. The surface downwelling longwave radiation (W/m^2) for 1) PPS and the differences 2) MSG-PPS 3) ECMWF-PPS 4) ECMWF-MSG 5) RCA-PPS 6) RCA-MSG for September, December 2005 and March, June 2006.

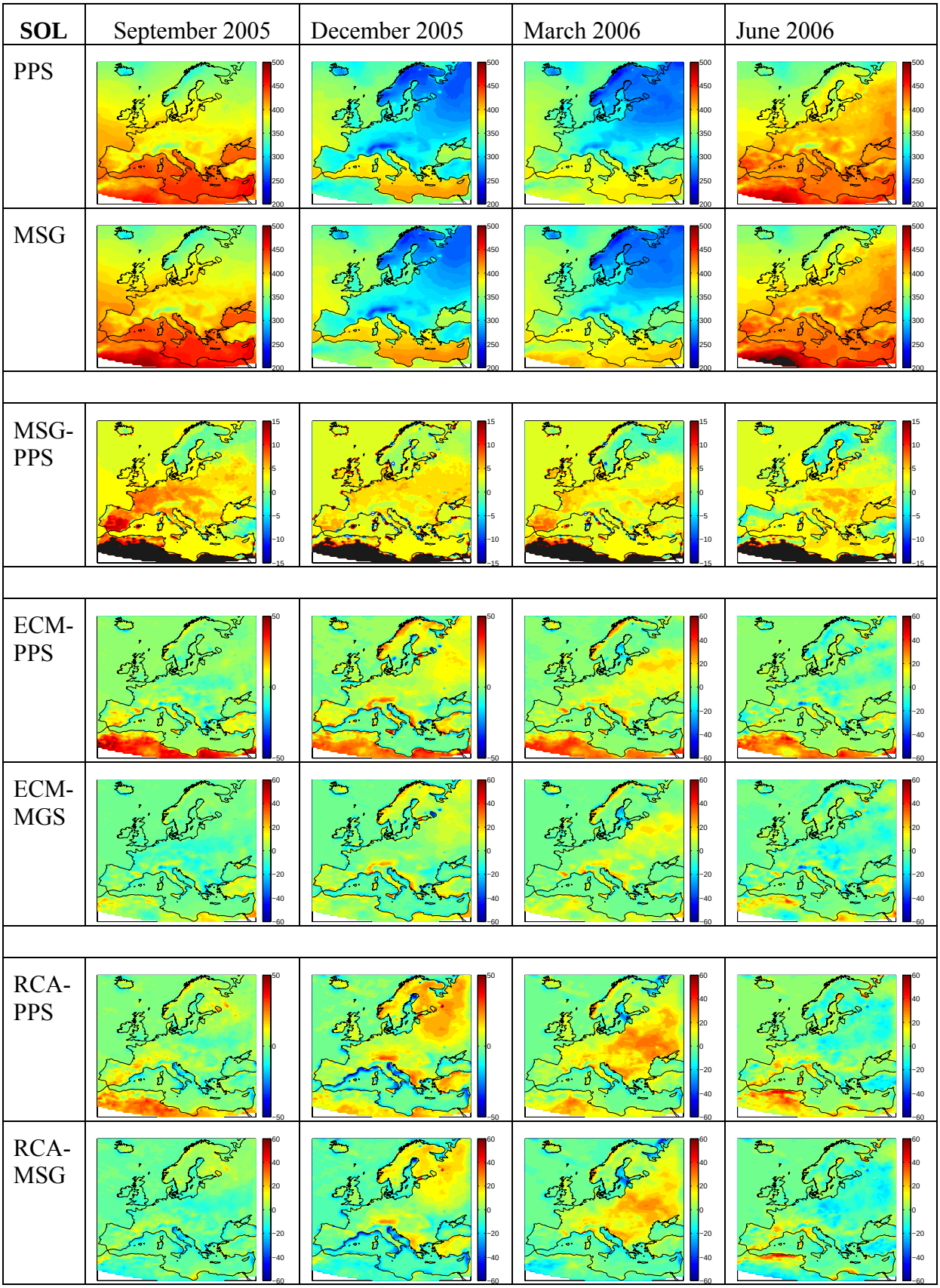

Figure 11. The surface outgoing longwave radiation (W/m^2) at the surface for 1) PPS and the differences 2) MSG-PPS 3) ECMWF-PPS 4) ECMWF-MSG 5) RCA-PPS 6) RCA-MSG for September, December 2005 and March, June 2006. Note the different scales for the MSG-PPS difference plots in row 3.

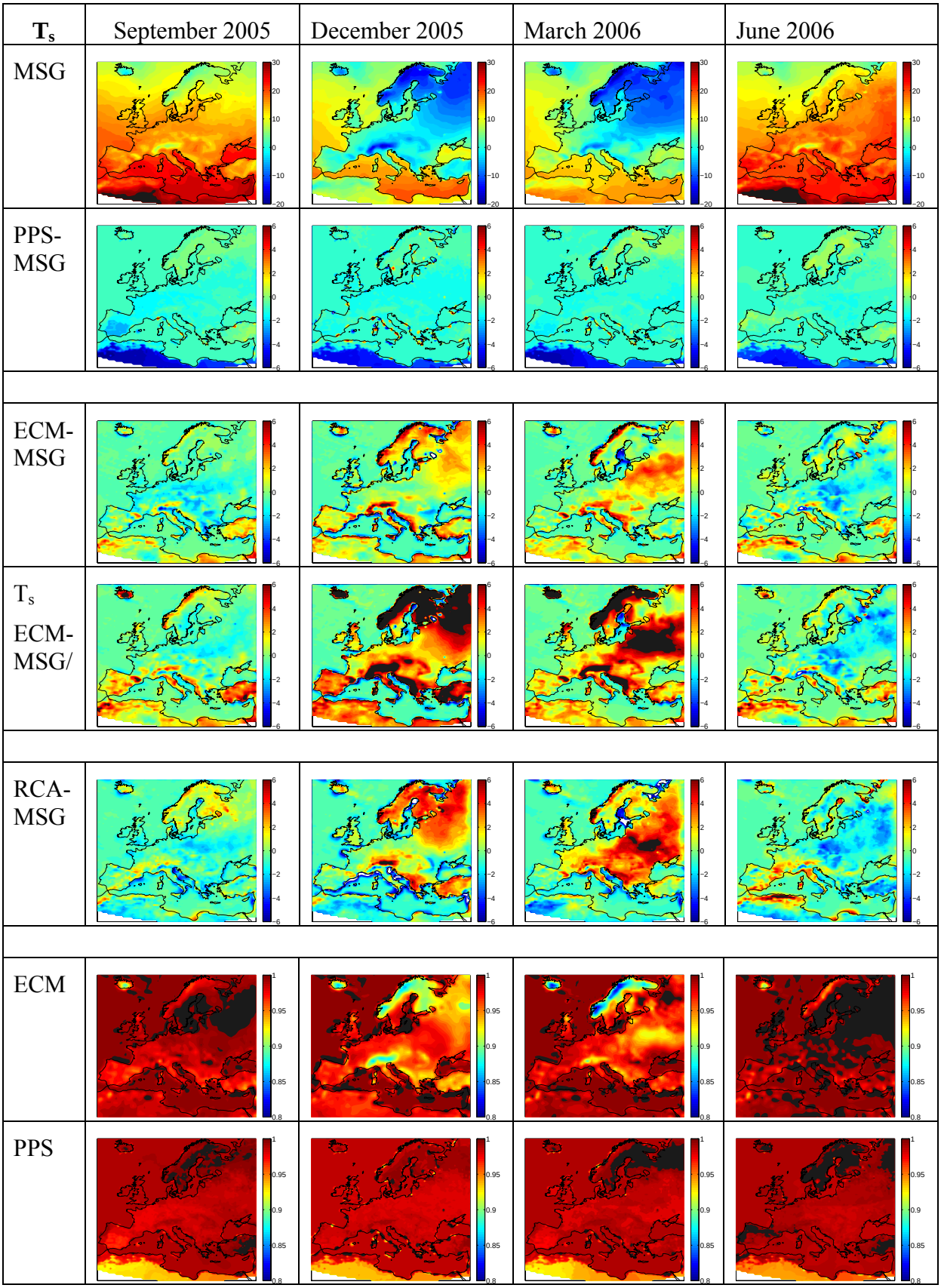

Figure 12. The calculated skin surface temperature T_s calculated for 1) MSG and the differences 2) PPS-MSG 3) ECMWF-MSG 4) ECMWF actual Ts-MSG 5) RCA-MSG and the emissivity for 6) ECMWF and 7) PPS for September, December 2005 and March, June 2006.

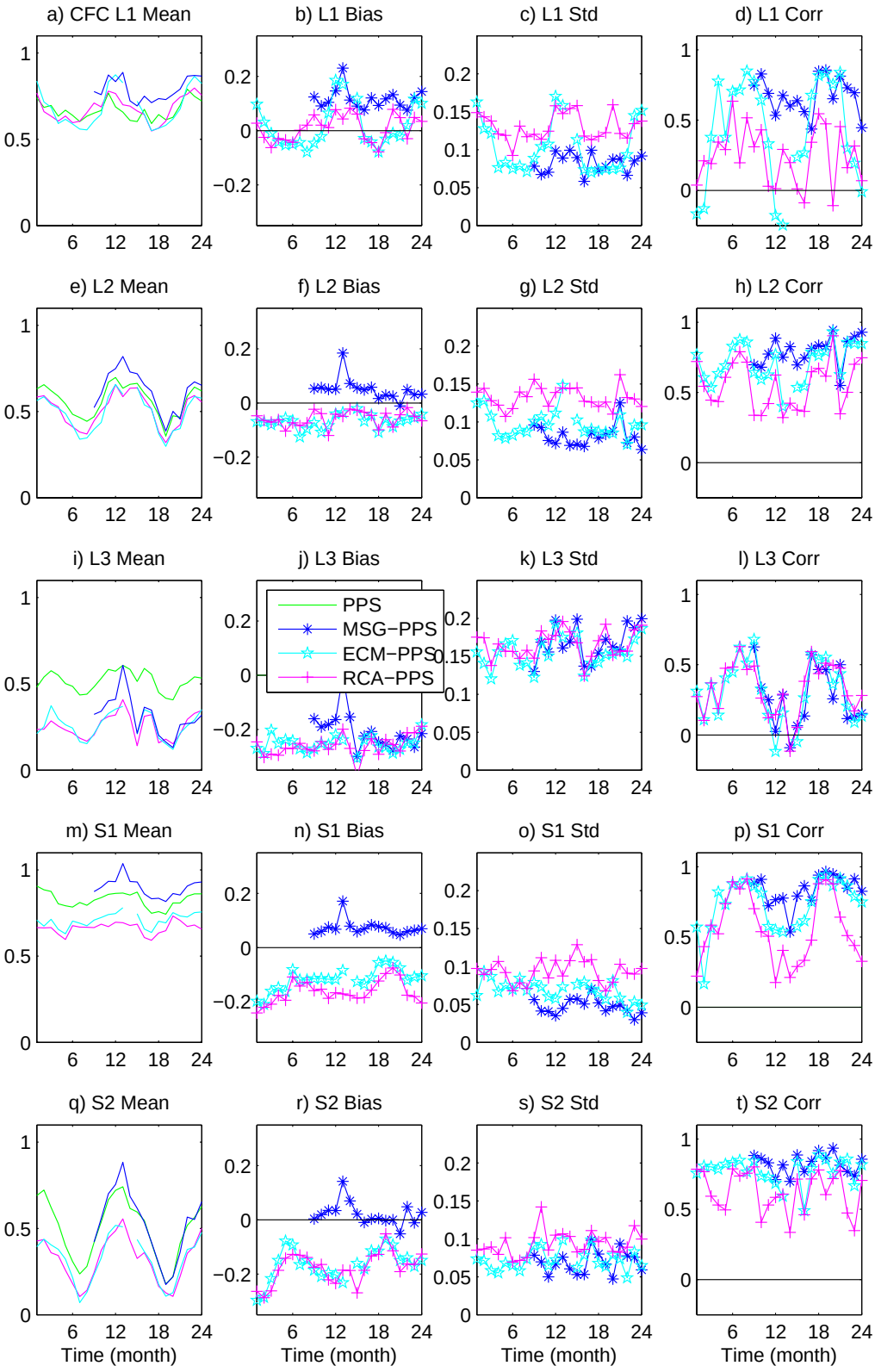

Figure 13. The mean cloud fraction for PPS, MSG, ECMWF and RCA for L1 (land points north of 53°N latitude), L2 (land points north of 36°N and south of 55°N latitude), L3 (land points south of 36°N latitude), S1 (sea points north of 43°N latitude) and S2 (sea points south of 43°N latitude) in the first column. The three other columns show the bias, standard deviation and correlation for MSG, ECMWF and RCA compared to PPS for the period January 2005 until December 2006.

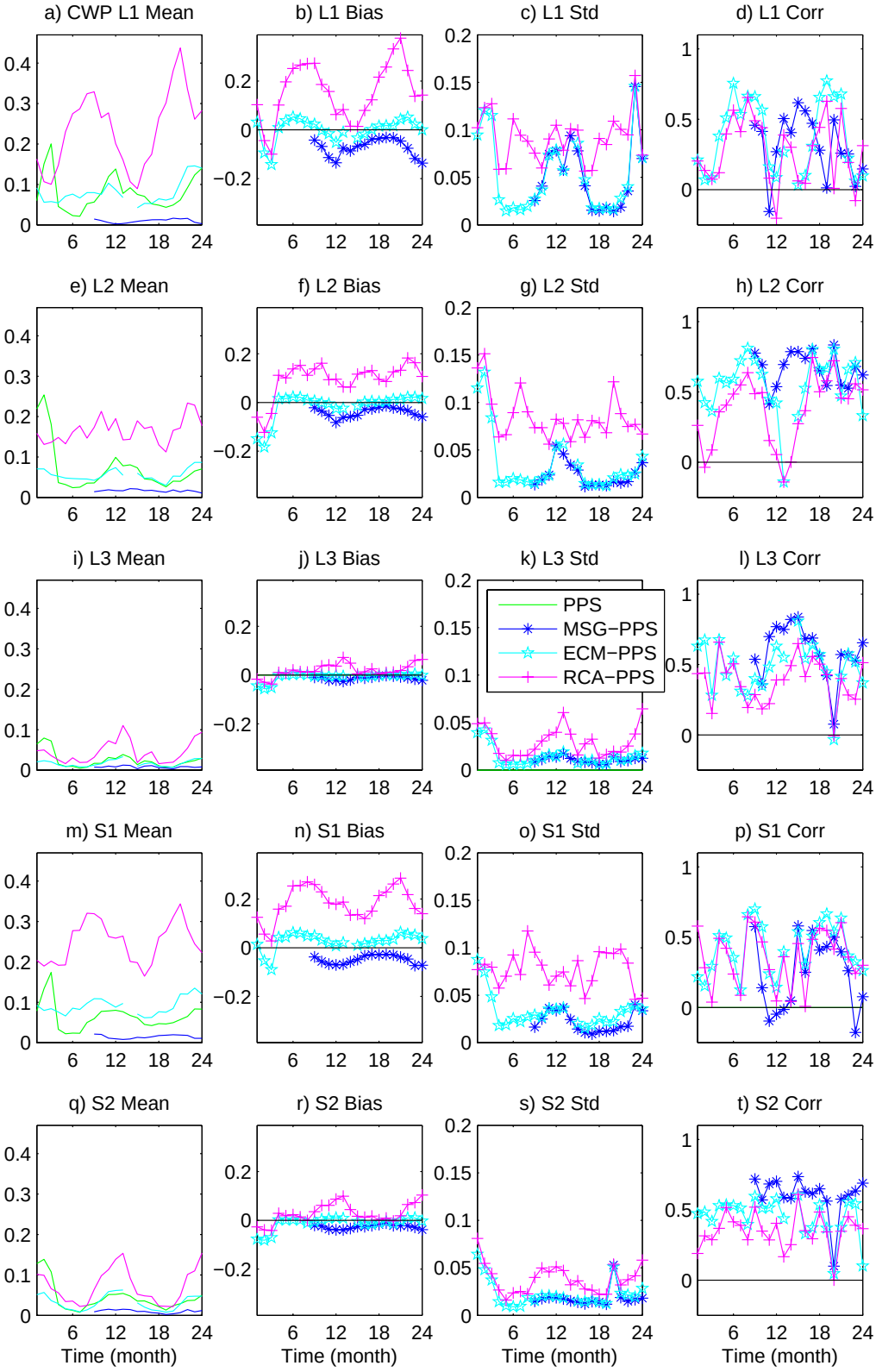

Figure 14. The cloud water path (kg/m2), same variables and regions as in Figure13.

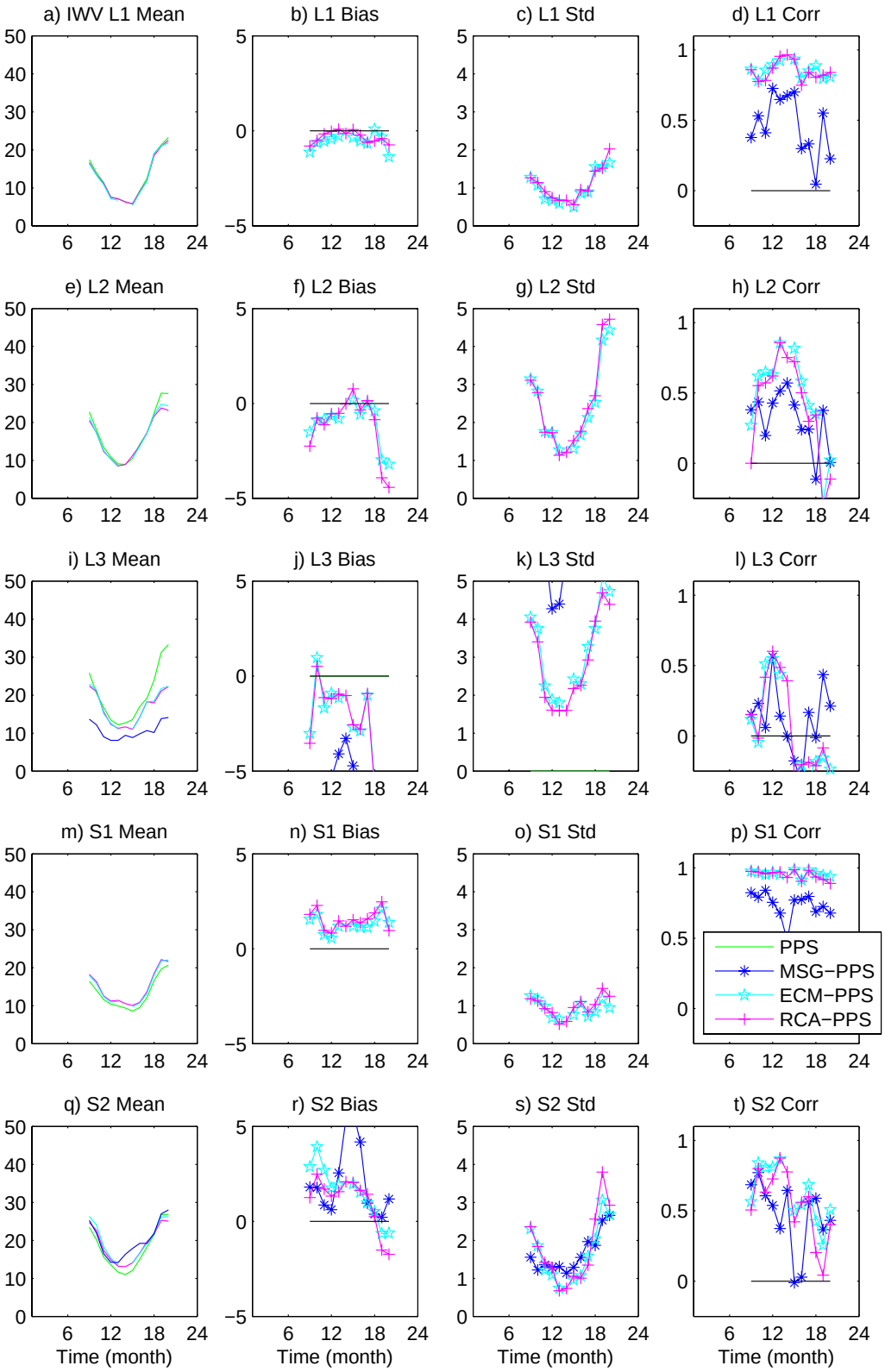

Figure 15. The vertically integrated water vapour (HTW or IWV) (kg/m^2), same variables and regions as in Figure13.

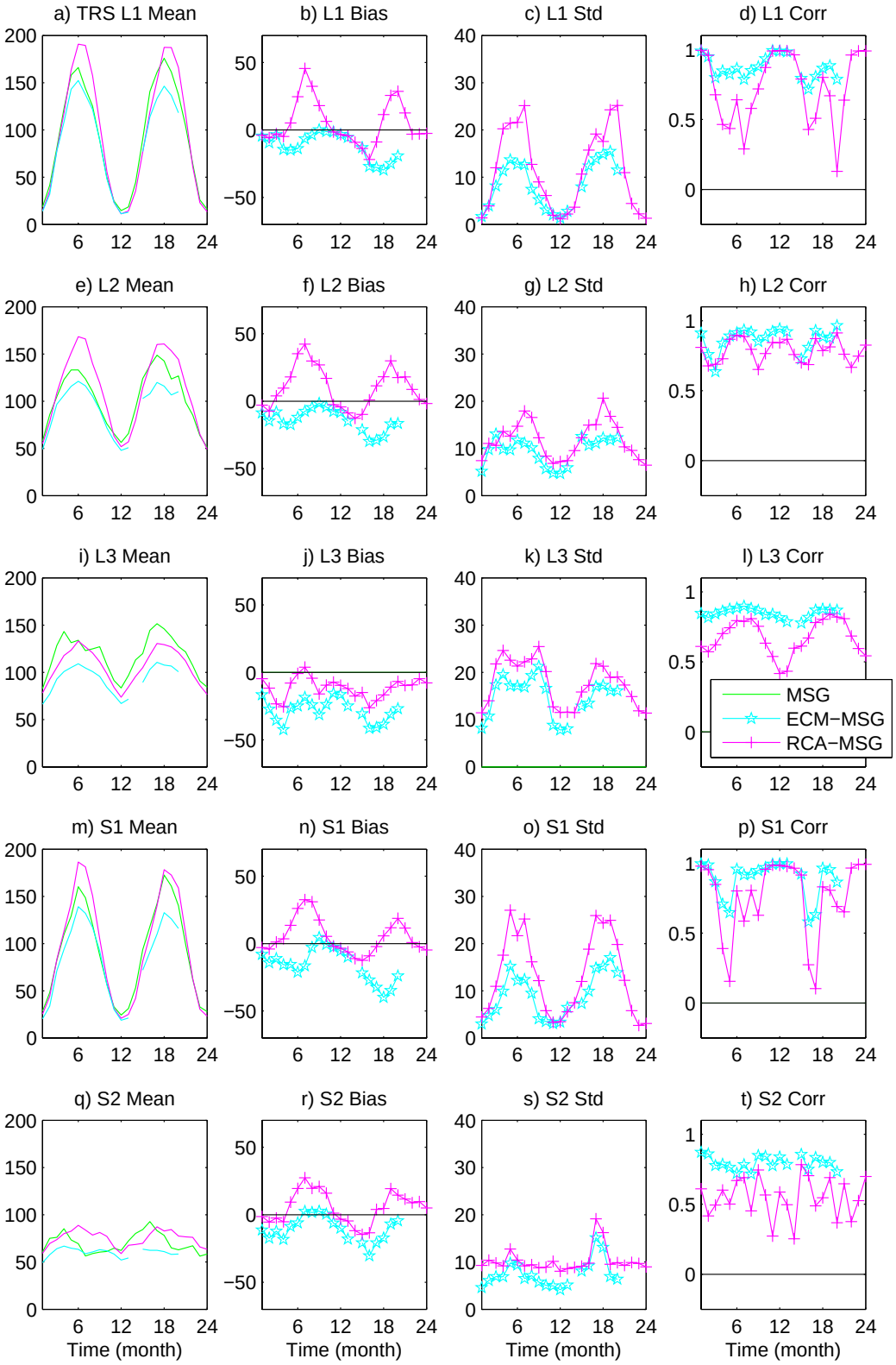

Figure 16. The TOA reflected solar radiation (W/m^2), same variables and regions as in Figure13.

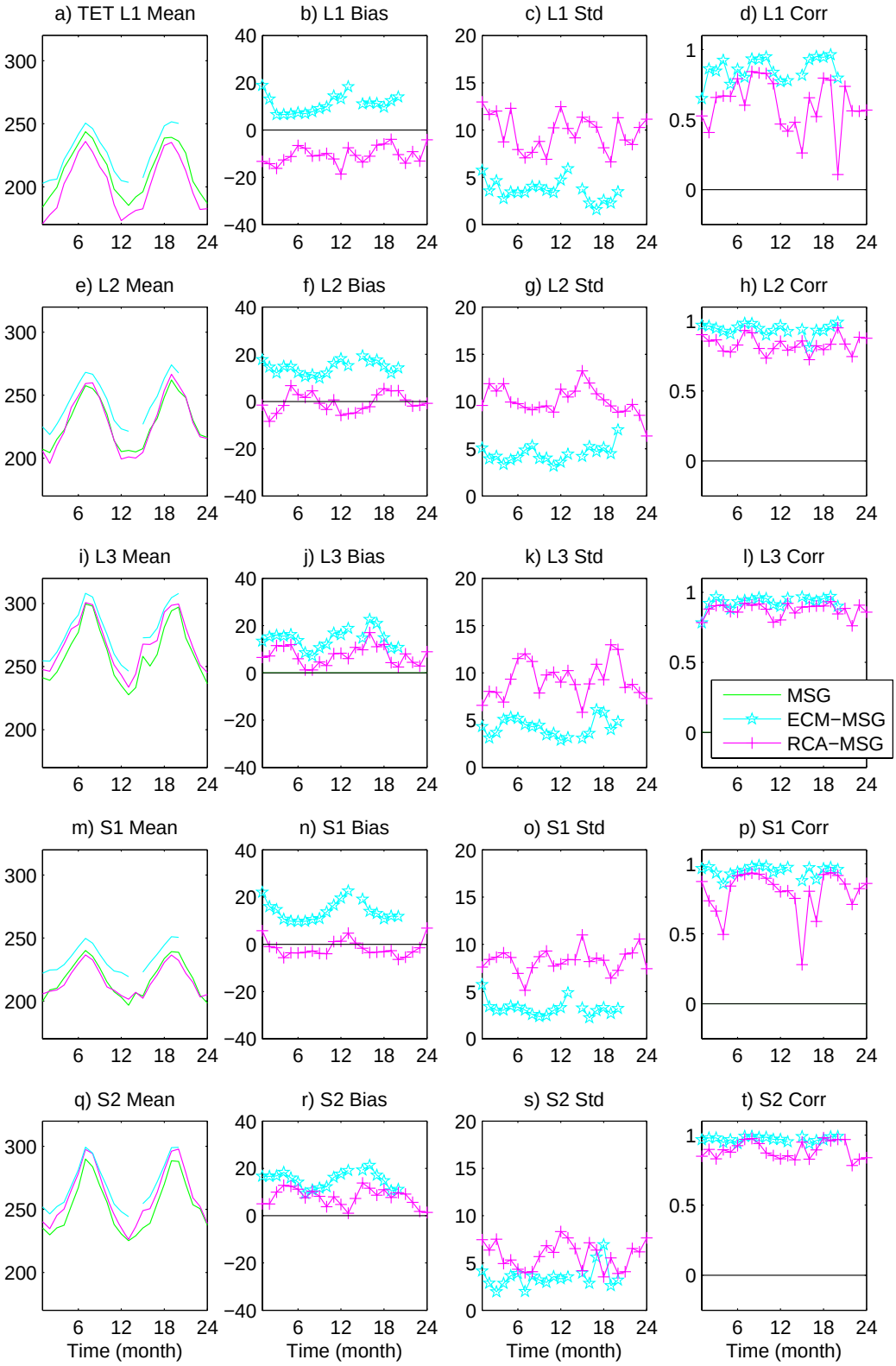

Figure 17. The TOA emitted thermal radiation (W/m^2), same variables and regions as in Figure13

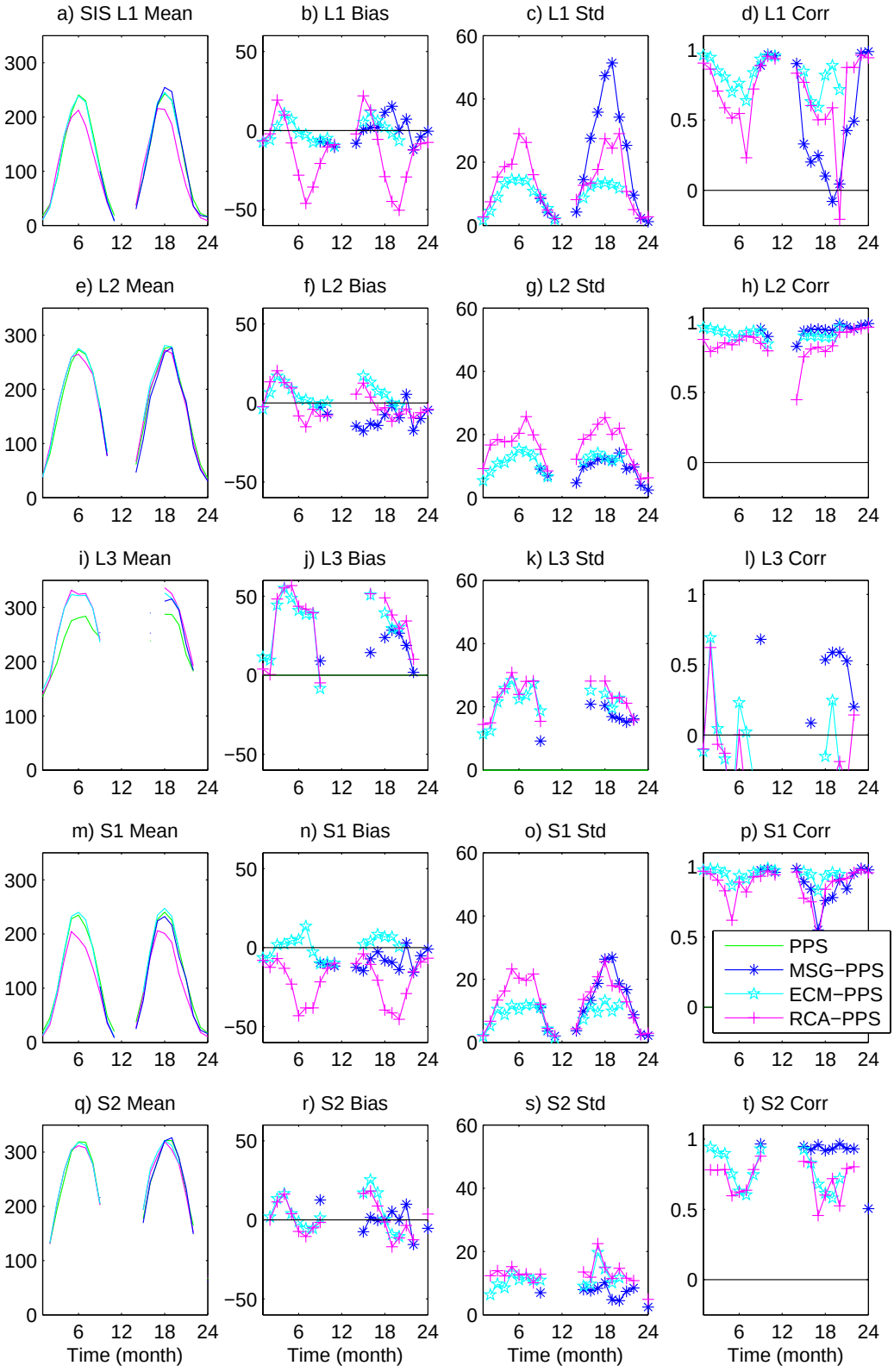

Figure 18. The surface incoming solar radiation (W/m^2), same variables and regions as in Figure13.

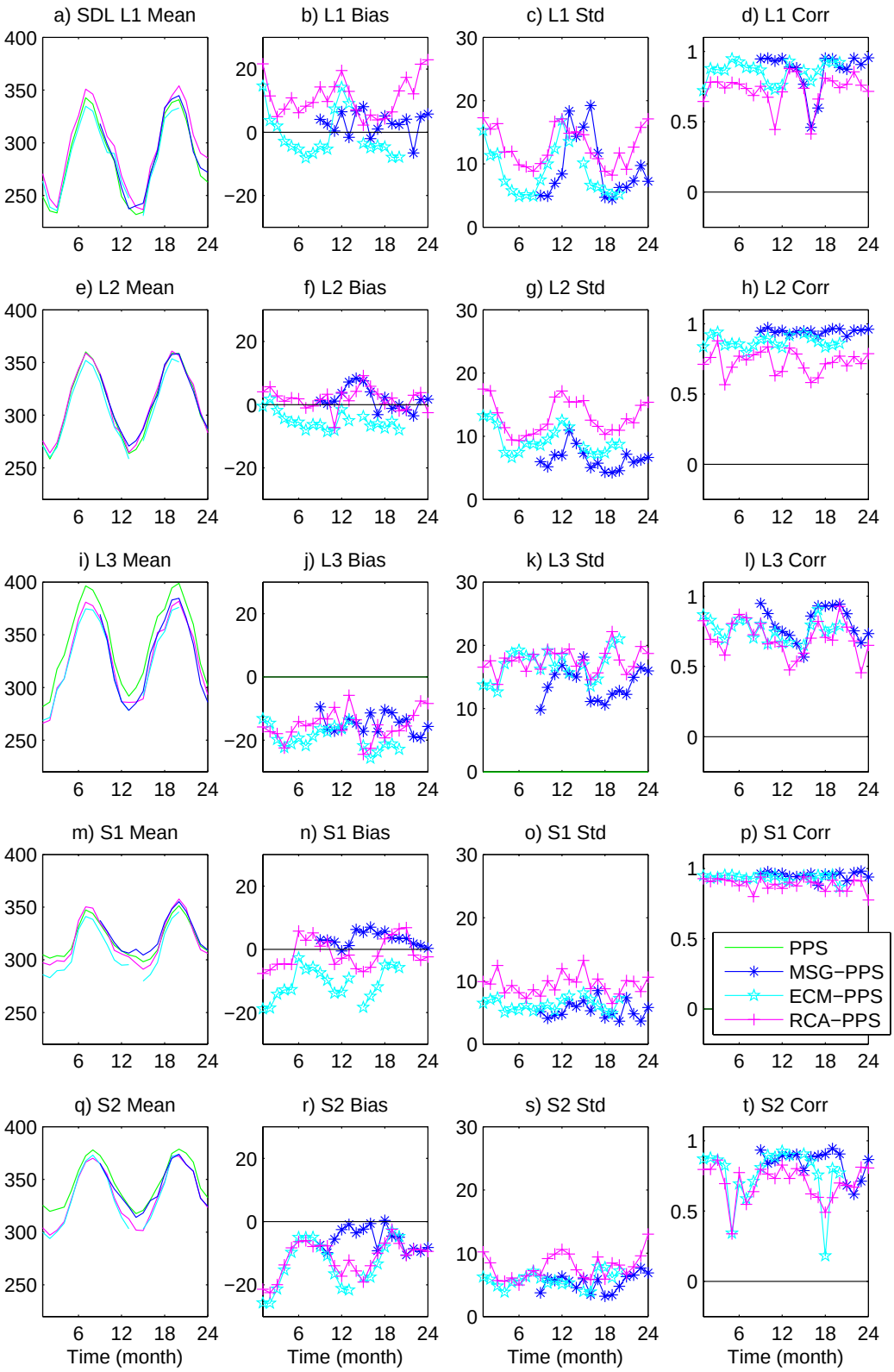

Figure 19. The surface downwelling longwave radiation (W/m^2), same variables and regions as in Figure13.

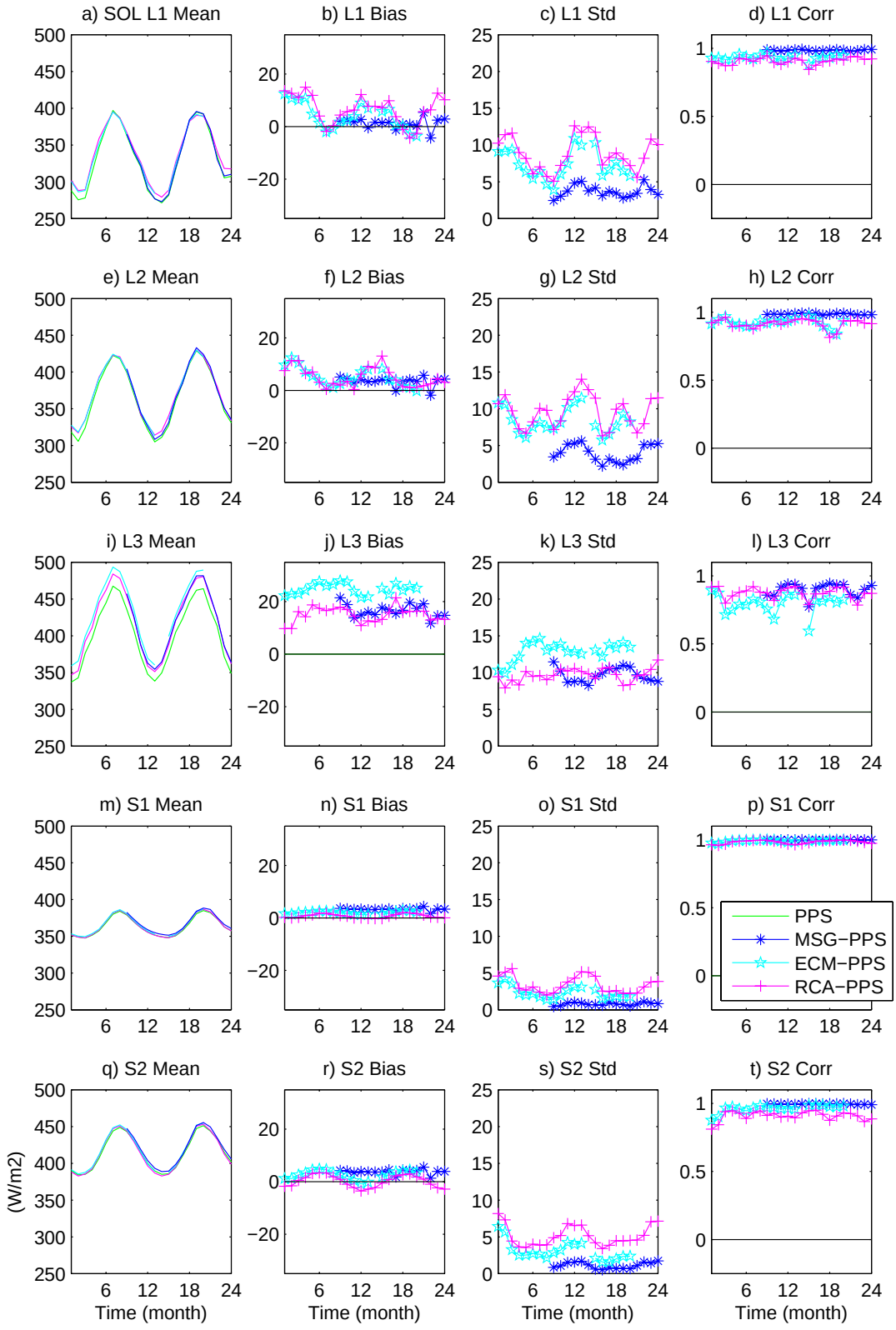

Figure 20. The surface outgoing longwave radiation (W/m^2), same variables and regions as in Figure13.

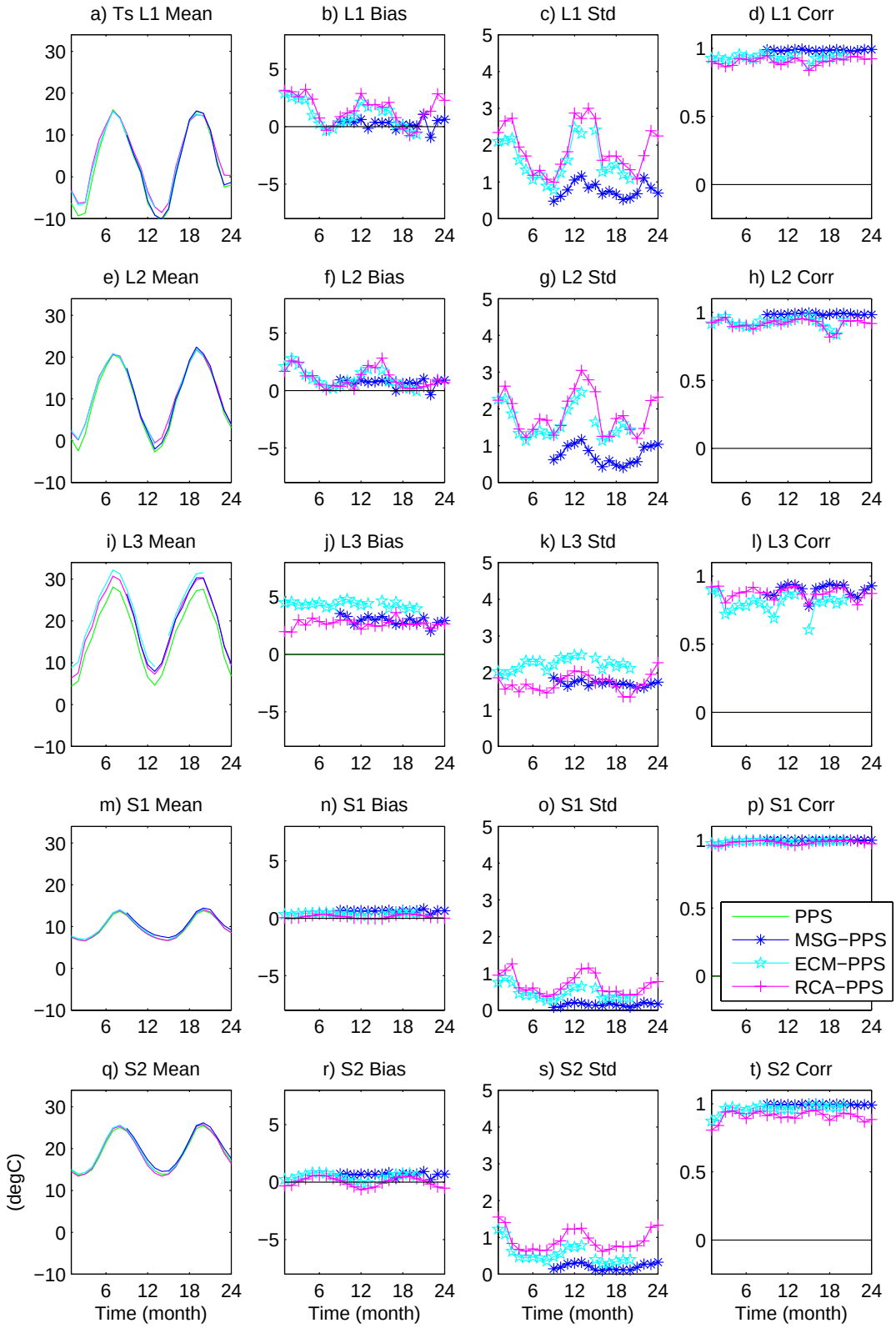

Figure 21. The calculated skin temperature (°C), same variables and regions as in Figure13.

SMHIs publiceringar

SMHI ger ut sex rapportserier. Tre av dessa, R-serierna är avsedda för internationell publik och skrivs därför oftast på engelska. I de övriga serierna används det svenska språket.

Seriernas namn	**Publiceras sedan**
RMK (Rapport Meteorologi och Klimatologi)	1974
RH (Rapport Hydrologi)	1990
RO (Rapport Oceanografi)	1986
METEOROLOGI	1985
HYDROLOGI	1985
OCEANOGRAFI	1985

I serien METEOROLOGI har tidigare utgivits:

1985

1 Hagmarker, A. (1985)
Satellitmeteorologi.

2 Fredriksson, U., Persson, Ch., Laurin, S. (1985)
Helsingborgsluft.

3 Persson, Ch., Wern, L. (1985)
Spridnings- och depositionsberäkningar för av fallsförbränningsanläggningar i Sofielund och Högdalen.

4 Kindell, S. (1985)
Spridningsberäkningar för SUPRAs anläggningar i Köping.

5 Andersson, C., Kvick, T. (1985)
Vindmätningar på tre platser på Gotland. Utvärdering nr 1.

6 Kindell, S. (1985)
Spridningsberäkningar för Ericsson, Ingelstafabriken.

7 Fredriksson, U. (1985)
Spridningsberäkningar för olika plymlyft vid avfallsvärmeverket Sävenäs.

8 Fredriksson, U., Persson, Ch. (1985)
NO_x- och NO_2-beräkningar vid Vasaterminalen i Stockholm.

9 Wern, L. (1985)
Spridningsberäkningar för ASEA transformers i Ludvika.

10 Axelsson, G., Eklind, R. (1985)
Ovädret på Östersjön 23 juli 1985.

11 Laurin, S., Bringfelt, B. (1985)
Spridningsmodell för kväveoxider i gatumiljö.

12 Persson, Ch., Wern, L. (1985)
Spridnings- och depositionsberäkningar för avfallsförbränningsanläggning i Sofielund.

13 Persson, Ch., Wern, L. (1985)
Spridnings- och depositionsberäkningar för avfallsförbränningsanläggning i Högdalen.

14 Vedin, H., Andersson, C. (1985)
Extrema köldperioder i Stockholm.

15 Krieg, R., Omstedt, G. (1985)
Spridningsberäkningar för Volvos planerade bilfabrik i Uddevalla.

16 Kindell, S. Wern, L. (1985)
Luftvårdsstudie avseende industrikombinatet i Nynäshamn (koncentrations- och luktberäkningar).

17 Laurin, S., Persson, Ch. (1985)
Beräknad formaldehydspridning och deposition från SWEDSPANs spånskivefabrik.

18 Persson, Ch., Wern, L. (1985)
Luftvårdsstudie avseende industri-kombinatet i Nynäshamn – depositions-beräkningar av koldamm.

19 Fredriksson, U. (1985)
Luktberäkningar för Bofors Plast i Ljungby, II.

20 Wern, L., Omstedt, G. (1985)
Spridningsberäkningar för Volvos planerade bilfabrik i Uddevalla - energicentralen.

21 Krieg, R., Omstedt, G. (1985)
Spridningsberäkningar för Volvos planerade bilfabrik i Uddevalla - kompletterande beräkningar för fabrikerna.

22 Karlsson, K.-G. (1985)
Information från Meteosat - forskningsrön och operationell tillämpning.

23 Fredriksson, U. (1985)
Spridningsberäkningar för AB Åkerlund & Rausings fabrik i Lund.

24 Färnlöf, S. (1985)
Radarmeteorologi.

25 Ahlström, B., Salomonsson, G. (1985)
Resultat av 5-dygnsprognos till ledning för isbrytarverksamhet vintern 1984-85.

26 Wern, L. (1985)
Avesta stadsmodell.

27 Hultberg, H. (1985)
Statistisk prognos av yttemperatur.

1986

1 Krieg, R., Johansson, L., Andersson, C. (1986)
Vindmätningar i höga master, kvartalsrapport 3/1985.

2 Olsson, L.-E., Kindell, S. (1986)
Air pollution impact assessment for the SABAH timber, pulp and paper complex.

3 Ivarsson, K.-I. (1986)
Resultat av byggväderprognoser - säsongen 1984/85.

4 Persson, Ch., Robertson, L. (1986)
Spridnings- och depositionsberäkningar för en sopförbränningsanläggning i Skövde.

5 Laurin, S. (1986)
Bilavgaser vid intagsplan - Eskilstuna.

6 Robertson, L. (1986)
Koncentrations- och depositionsberäkningar för en sopförbränningsanläggning vid Ryaverken i Borås.

7 Laurin, S. (1986)
Luften i Avesta - föroreningsbidrag från trafiken.

8 Robertson, L., Ring, S. (1986)
Spridningsberäkningar för bromcyan.

9 Wern, L. (1986)
Extrema byvindar i Orrefors.

10 Robertson, L. (1986)
Koncentrations- och depositionsberäkningar för Halmstads avfallsförbränningsanläggning vid Kristinehed.

11 Törnevik, H., Ugnell (1986)
Belastningsprognoser.

12 Joelsson, R. (1986)
Något om användningen av numeriska prognoser på SMHI (i princip rapporten till ECMWF).

13 Krieg, R., Andersson, C. (1986)
Vindmätningar i höga master, kvartalsrapport 4/1985.

14 Dahlgren, L. (1986)
Solmätning vid SMHI.

15 Wern, L. (1986)
Spridningsberäkningar för ett kraftvärmeverk i Sundbyberg.

16 Kindell, S. (1986)
Spridningsberäkningar för Uddevallas fjärrvärmecentral i Hovhult.

17 Häggkvist, K., Persson, Ch., Robertson, L (1986)
Spridningsberäkningar rörande gasutsläpp från ett antal källor inom SSAB Luleåverken.

18 Krieg, R., Wern, L. (1986)
En klimatstudie för Arlanda stad.

19 Vedin, H. (1986)
Extrem arealnederbörd i Sverige.

20 Wern, L. (1986)
Spridningsberäkningar för lösningsmedel i Tibro.

21 Krieg, R., Andersson, C. (1986)
Vindmätningar i höga master - kvartalsrapport 1/1986.

22 Kvick, T. (1986)
Beräkning av vindenergitillgången på några platser i Halland och Bohuslän.

23 Krieg, R., Andersson, C. (1986)
Vindmätningar i höga master - kvartalsrapport 2/1986.

24 Persson, Ch. (SMHI), Rodhe, H. (MISU), De Geer, L.-E. (FOA) (1986)
Tjernobylolyckan - En meteorologisk analys av hur radioaktivitet spreds till Sverige.

25 Fredriksson, U. (1986)
Spridningsberäkningar för Spendrups bryggeri, Grängesberg.

26 Krieg, R. (1986)
Beräkningar av vindenergitillgången på några platser i Skåne.

27 Wern, L., Ring, S. (1986)
Spridningsberäkningar, SSAB.

28 Wern, L., Ring, S. (1986)
Spridningsberäkningar för ny ugn, SSAB II.

29 Wern, L. (1986)
Spridningsberäkningar för Volvo Hallsbergverken.

30 Fredriksson, U. (1986)
SO_2-halter från Hammarbyverket kring ny arena vid Johanneshov.

31 Persson, Ch., Robertson, L., Häggkvist, K. (1986)
Spridningsberäkningar, SSAB - Luleåverken.

32 Kindell, S., Ring, S. (1986)
Spridningsberäkningar för SAABs planerade bilfabrik i Malmö.

33 Wern, L. (1986)
Spridningsberäkningar för svavelsyrafabrik i Falun.

34 Wern, L., Ring, S. (1986)
Spridningsberäkningar för Västhamnsverket HKV1 i Helsingborg.

35 Persson, Ch., Wern, L. (1986)
Beräkningar av svaveldepositionen i Stockholmsområdet.

36 Joelsson, R. (1986)
USAs månadsprognoser.

37 Vakant nr.

38 Krieg, R., Andersson, C. (1986)
Utemiljön vid Kvarnberget, Lysekil.

39 Häggkvist, K. (1986)
Spridningsberäkningar av freon 22 från Ropstens värmepumpverk.

40 Fredriksson, U. (1986)
Vindklassificering av en plats på Hemsön.

41 Nilsson, S. (1986)
Utvärdering av sommarens (1986) använda konvektionsprognoshjälpmedel.

42 Krieg, R., Kvick, T. (1986)
Vindmätningar i höga master.

43 Krieg, R., Fredriksson, U. (1986)
Vindarna över Sverige.

44 Robertson, L. (1986)
Spridningsberäkningar rörande gasutsläpp vid ScanDust i Landskrona - bestämning av cyanvätehalter.

45 Kvick, T., Krieg, R., Robertson, L. (1986)
Vindförhållandena i Sveriges kust- och havsband, rapport nr 2.

46 Fredriksson, U. (1986)
Spridningsberäkningar för en planerad panncentral vid Lindsdal utanför Kalmar.

47 Fredriksson, U. (1986)
Spridningsberäkningar för Volvo BMs fabrik i Landskrona.

48 Fredriksson, U. (1986)
Spridningsberäkningar för ELMO-CALFs fabrik i Svenljunga.

49 Häggkvist, K. (1986)
Spridningsberäkningar rörande gasutsläpp från syrgas- och bensenupplag inom SSAB Luleåverken.

50 Wern, L., Fredriksson, U., Ring, S. (1986)
Spridningsberäkningar för lösningsmedel i Tidaholm.

51 Wern, L. (1986)
Spridningsberäkningar för Volvo BM ABs anläggning i Braås.

52 Ericson, K. (1986)
Meteorological measurements performed May 15, 1984, to June, 1984, by the SMHI.

53 Wern, L., Fredriksson, U. (1986)
Spridningsberäkning för Kockums Plåtteknik, Ronneby.

54 Eriksson, B. (1986)
Frekvensanalys av timvisa temperaturobservationer.

55 Wern, L., Kindell, S. (1986)
Luktberäkningar för AB ELMO i Flen.

56 Robertson, L. (1986)
Spridningsberäkningar rörande utsläpp av NO_x inom Fagersta kommun.

57 Kindell, S. (1987)
Luften i Nässjö.

58 Persson, Ch., Robertson, L. (1987)
Spridningsberäkningar rörande gasutsläpp vid ScanDust i Landskrona - bestämning av cyanväte.

59 Bringfelt, B. (1987)
Receptorbaserad partikelmodell för gatumiljömodell för en gata i Nyköping.

60 Robertson, L. (1987)
Spridningsberäkningar för Varbergs kommun. Bestämning av halter av SO_2, CO, NO_x samt några kolväten.

61 Vedin, H., Andersson, C. (1987)
E 66 - Linderödsåsen - klimatförhållanden.

62 Wern, L., Fredriksson, U. (1987)
Spridningsberäkningar för Kockums Plåtteknik, Ronneby. 2.

63 Taesler, R., Andersson, C., Wallentin, C., Krieg, R. (1987)
Klimatkorrigering för energiförbrukningen i ett eluppvärmt villaområde.

64 Fredriksson, U. (1987)
Spridningsberäkningar för AB Åetå-Trycks planerade anläggning vid Kungens Kurva.

65 Melgarejo, J. (1987)
Mesoskalig modellering vid SMHI.

66 Häggkvist, K. (1987)
Vindlaster på kordahus vid Alviks Strand - numeriska beräkningar.

67 Persson, Ch. (1987)
Beräkning av lukt och föroreningshalter i luft runt Neste Polyester i Nol.

68 Fredriksson, U., Krieg, R. (1987)
En överskalig klimatstudie för Tornby, Linköping.

69 Häggkvist, K. (1987)
En numerisk modell för beräkning av vertikal momentumtransport i områden med stora råhetselement. Tillämpning på ett energiskogsområde.

70 Lindström, Kjell (1987)
Weather and flying briefing aspects.

71 Häggkvist, K. (1987)
En numerisk modell för beräkning av vertikal momentumtransport i områden med stora råhetselement. En koefficientbestämning.

72 Liljas, E. (1988)
Förbättrad väderinformation i jordbruket - behov och möjligheter (PROFARM).

73 Andersson, Tage (1988)
Isbildning på flygplan.

74 Andersson, Tage (1988)
Aeronautic wind shear and turbulence.
A review for forecasts.

75 Källberg, P. (1988)
Parameterisering av diabatiska processer i numeriska prognosmodeller.

76 Vedin, H., Eriksson, B. (1988)
Extrem arealnederbörd i Sverige 1881 - 1988.

77 Eriksson, B., Carlsson, B., Dahlström, B. (1989)
Preliminär handledning för korrektion av nederbördsmängder.

78 Liljas, E. (1989)
Torv-väder. Behovsanalys med avseende på väderprognoser och produktion av bränsletorv.

79 Hagmarker, A. (1991)
Satellitmeteorologi.

80 Lövblad, G., Persson, Ch. (1991)
Background report on air pollution situation in the Baltic states - a prefeasibility study.
IVL Publikation B 1038.

81 Alexandersson, H., Karlström, C., Larsson-McCann, S. (1991)
Temperaturen och nederbörden i Sverige 1961-90. Referensnormaler.

82 Vedin, H., Alexandersson, H., Persson, M. (1991)
Utnyttjande av persistens i temperatur och nederbörd för vårflödesprognoser.

83 Moberg, A. (1992)
Lufttemperaturen i Stockholm 1756 - 1990. Historik, inhomogeniteter och urbaniseringseffekt.
Naturgeografiska Institutionen, Stockholms Universitet.

84 Josefsson, W. (1993)
Normalvärden för perioden 1961-90 av globalstrålning och solskenstid i Sverige.

85 Laurin, S., Alexandersson, H. (1994)
Några huvuddrag i det svenska temperatur-klimatet 1961 - 1990.

86 Fredriksson, U. och Ståhl, S. (1994)
En jämförelse mellan automatiska och manuella fältmätningar av temperatur och nederbörd.

87 Alexandersson, H., Eggertsson Karlström, C. och Laurin S. (1997).
Några huvuddrag i det svenska nederbördsklimatet 1961-1990.

88 Mattsson, J., Rummukainen, M. (1998)
Växthuseffekten och klimatet i Norden - en översikt.

89 Kindbom, K., Sjöberg, K., Munthe, J., Peterson, K. (IVL)
Persson, C. Roos, E., Bergström, R. (SMHI). (1998)
Nationell miljöövervakning av luft- och nederbördskemi 1996.

90 Foltescu, V.L., Häggmark, L (1998)
Jämförelse mellan observationer och fält med griddad klimatologisk information.

91 Hultgren, P., Dybbroe, A., Karlsson, K.-G. (1999)
SCANDIA – its accuracy in classifying LOW CLOUDS

92 Hyvarinen, O., Karlsson, K.-G., Dybbroe, A. (1999)
Investigations of NOAA AVHRR/3 1.6 μm imagery for snow, cloud and sunglint discrimination (Nowcasting SAF)

93 Bennartz, R., Thoss, A., Dybbroe, A. and Michelson, D. B. (1999)
Precipitation Analysis from AMSU (Nowcasting SAF)

94 Appelqvist, Peter och Anders Karlsson (1999)
Nationell emissionsdatabas för utsläpp till luft - Förstudie.

95 Persson, Ch., Robertson L. (SMHI)
Thaning, L (LFOA). (2000)
Model for Simulation of Air and Ground Contamination Associated with Nuclear Weapons. An Emergency Preparedness Model.

96 Kindbom K., Svensson A., Sjöberg K., (IVL) Persson C., (SMHI) (2001)
Nationell miljöövervakning av luft- och nederbördskemi 1997, 1998 och 1999.

97 Diamandi, A., Dybbroe, A. (2001)
Nowcasting SAF
Validation of AVHRR cloud products.

98 Foltescu V. L., Persson Ch. (2001)
Beräkningar av moln- och dimdeposition i Sverigemodellen - Resultat för 1997 och 1998.

99 Alexandersson, H. och Eggertsson Karlström, C (2001)
Temperaturen och nederbörden i Sverige 1961-1990. Referensnormaler - utgåva 2.

100 Korpela, A., Dybbroe, A., Thoss, A. (2001)
Nowcasting SAF - Retrieving Cloud Top Temperature and Height in Semi-transparent and Fractional Cloudiness using AVHRR.

101 Josefsson, W. (1989)
Computed global radiation using interpolated, gridded cloudiness from the MESA-BETA analysis compared to measured global radiation.

102 Foltescu, V., Gidhagen, L., Omstedt, G. (2001)
Nomogram för uppskattning av halter av PM_{10} och NO_2

103 Omstedt, G., Gidhagen, L., Langner, J. (2002)
Spridning av förbränningsemissioner från småskalig biobränsleeldning
– analys av PM2.5 data från Lycksele med hjälp av två Gaussiska spridningsmodeller.

104 Alexandersson, H. (2002)
Temperatur och nederbörd i Sverige 1860 - 2001

105 Persson, Ch. (2002)
Kvaliteten hos nederbördskemiska mätdata

som utnyttjas för dataassimilation i MATCH-Sverige modellen".

106 Mattsson, J., Karlsson, K-G. (2002)
CM-SAF cloud products feasibility study in the inner Arctic region
Part I: Cloud mask studies during the 2001 Oden Arctic expedition

107 Kärner, O., Karlsson, K-G. (2003)
Climate Monitoring SAF - Cloud products feasibility study in the inner Arctic region.
Part II: Evaluation of the variability in radiation and cloud data

108 Persson, Ch., Magnusson, M. (2003)
Kvaliteten i uppmätta nederbördsmängder inom svenska nederbörskemiska stationsnät

109 Omstedt, G., Persson Ch., Skagerström, M (2003)
Vedeldning i småhusområden

110 Alexandersson, H., Vedin, H. (2003)
Dimensionerande regn för mycket små avrinningsområden

111 Alexandersson, H. (2003)
Korrektion av nederbörd enligt enkel klimatologisk metodik

112 Joro, S., Dybbroe, A.(2004)
Nowcasting SAF – IOP
Validating the AVHRR Cloud Top Temperature and Height product using weather radar data
Visiting Scientist report

113 Persson, Ch., Ressner, E., Klein, T. (2004)
Nationell miljöövervakning – MATCH-Sverige modellen
Metod- och resultatsammanställning för åren 1999-2002 samt diskussion av osäkerheter, trender och miljömål

114 Josefsson, W. (2004)
UV-radiation measured in Norrköping 1983-2003.

115 Martin, Judit, (2004)
Var tredje timme – Livet som väderobservatör

116 Gidhagen, L., Johansson, C., Törnquist, L. (2004)
NORDIC – A database for evaluation of dispersion models on the local, urban and regional scale

117 Langner, J., Bergström, R., Klein, T., Skagerström, M. (2004)
Nuläge och scenarier för inverkan på marknära ozon av emissioner från Västra Götalands län – Beräkningar för 1999

118 Trolez, M., Tetzlaff, A., Karlsson, K-G. (2005)
CM-SAF Validating the Cloud Top Height product using LIDAR data

119 Rummukainen, M. (2005)
Växthuseffekten

120 Omstedt, G. (2006)
Utvärdering av PM_{10} - mätningar i några olika nordiska trafikmiljöer

121 Alexandersson, H. (2006)
Vindstatistik för Sverige 1961-2004

122 Samuelsson, P., Gollvik, S., Ullerstig, A., (2006)
The land-surface scheme of the Rossby Centre regional atmospheric climate model (RCA3)

123 Omstedt, G. (2007)
VEDAIR – ett internetverktyg för beräkning av luftkvalitet vid småskalig biobränsleeldning
Modellbeskrivning och slutrapport mars 2007

124 Persson, G., Strandberg, G., Bärring, L., Kjellström, E. (2007)
Beräknade temperaturförhållanden för tre platser i Sverige – perioderna 1961-1990 och 2011-2040

125 Engart, M., Foltescu, V. (2007)
Luftföroreningar i Europa under framtida klimat

126 Jansson, A., Josefsson, W. (2007)
Modelling of surface global radiation and CIE-weighted UV-radiation for the period 1980-2000

127 Johnston, S., Karlsson, K-G. (2007)
METEOSAT 8 SEVIRI and NOAA Cloud Products. A Climate Monitoring SAF Comparison Study

128 Eliasson, S., Tetzlaf, A., Karlsson, K-G. (2007)
Prototyping an improved PPS cloud detection for the Arctic polar night

129 Trolez, M., Karlsson, K-G., Johnston, S., Albert, P (2008)
The impact of varying NWP background information on CM-SAF cloud products

130 Josefsson, W., Löfvenius Ottosson, M. (2008)
Total ozone from zenith radiance measurements. An empirical model approach

Sveriges meteorologiska och hydrologiska institut
601 76 Norrköping · Tel 011-495 8000 · Fax 011-495 8001
www.smhi.se

ISSN 0283-7730